Magnetic nanostructures for emerging biomedical applications

Cite as: Appl. Phys. Rev. **7**, 011310 (2020); https://doi.org/10.1063/1.5121702
Submitted: 30 July 2019 . Accepted: 04 December 2019 . Published Online: 28 January 2020

L. Peixoto, R. Magalhães, D. Navas, S. Moraes, C. Redondo, R. Morales, J. P. Araújo, and C. T. Sousa

Applied Physics Reviews REVIEW scitation.org/journal/are

Magnetic nanostructures for emerging biomedical applications

Cite as: Appl. Phys. Rev. 7, 011310 (2020); doi: 10.1063/1.5121702
Submitted: 30 July 2019 · Accepted: 4 December 2019 ·
Published Online: 28 January 2020

View Online Export Citation CrossMark

L. Peixoto,[1] R. Magalhães,[1] D. Navas,[1,2] S. Moraes,[1] C. Redondo,[3] R. Morales,[4,5] J. P. Araújo,[1] and C. T. Sousa[1,a)]

AFFILIATIONS

[1]IFIMUP-Faculdade de Ciências da Universidade do Porto, Rua do Campo Alegre, 4169-007 Porto, Portugal
[2]Instituto de Ciencia de Materiales de Madrid, ICMM-CSIC, Sor Juana Inés de la Cruz 3, 28049 Madrid, Spain
[3]UPV-Dpto. de Química-Física, Universidad del País Vasco UPV/EHU, 48940 Leioa, Spain
[4]Dpto. de Química-Física & BCMaterials, Universidad del País Vasco UPV/EHU, 48940 Leioa, Spain
[5]IKERBASQUE, Basque Foundation for Science, 48011 Bilbao, Spain

[a)]Electronic mail: celiasousa@fc.up.pt

ABSTRACT

Magnetic nanostructures have been widely studied due to their potential applicability into several research fields such as data storage, sensing and biomedical applications. Focusing on the biomedical aspect, some new approaches deserve to be mentioned: cell manipulation and separation, contrast-enhancing agents for magnetic resonance imaging, and magnetomechanically induced cell death. This work focuses on understanding three different magnetic nanostructures, disks in the vortex state, synthetic antiferromagnetic particles and nanowires, first, by explaining their interesting properties and how they behave under an applied external field, before reviewing their potential applications for each of the aforementioned techniques.

TABLE OF CONTENTS

I. INTRODUCTION

During the last few decades, the advances in both synthesis and characterization techniques have opened up amazing possibilities to achieve magnetic nanostructures with well-controlled magnetic behaviors. Due to this versatility, nanoscale magnetic objects have been successfully used in a wide range of technological applications[1,2] such as in data storage, energy, and sensing.[3–17] Moreover and although one-dimensional (1D) and two-dimensional (2D) systems have been usually studied, it was recently demonstrated that three-dimensional (3D) nanostructures with new magnetic effects can also be prepared and explored.[18] Regarding the biomedical applications, main research has been focused on using magnetic nanoparticles (MNPs) that have been chemically synthesized with a normally, spherical shape.[19–21] As MNPs can be moved by an external magnetic field, they have been used in magnetic separation and drug or gene delivery.[22–26] Also, MNPs generate local magnetic fields that have been used in cancer diagnostics by detection of functionalized MNPs via giant magnetoresistance (GMR) sensors[16,27,28] and as a contrast agent to improve magnetic resonance imaging (MRI).[24,29,30] Finally, the third main application of MNPs has been the annihilation of cancer cells by hyperthermia and based on the concept that MNPs heated the local environment when external alternating magnetic fields were applied.[31–33] Therefore, MNPs, in combination with external applied magnetic fields, can be placed at the desired location, react with the local environment and locally perturb it, such as by delivering heat. In order to fulfill these requirements, one key issue is related to the fact that MNPs usually agglomerate forming clusters. In order to avoid the

clustering of MNPs in living bodies, it is desired that MNPs only exhibit magnetic moment upon the application of external magnetic fields while null magnetic moment at zero external applied magnetic field. For this reason, most of the research studies have been performed using MNPs in the superparamagnetic state, which can be exclusively achieved for particles with diameters not larger than a few nanometers. More recently, different kinds of magnetic nanostructures (MNSs), prepared using template-assisted methodologies, have been suggested. For example, MNSs in the vortex state[34] or synthetic antiferromagnetic MNSs[35] with no magnetic moment at remanence, equivalent to the superparamagnetic MNP, have shown promising results in cell separation, as a contrast-enhancing agent in MRI and in magnetomechanically induced cell damage. In contrast to the more traditional MNP fabrication processes based on chemical synthesis, MNSs can be produced using self-assembled or lithographed templates in combination with physical vapor deposition and/or electrodeposition techniques. MNSs are very versatile and have some advantages with respect to MNPs:

1. Depending on the template geometry and the deposition technique, MNSs can show different geometries, such as disks, rods, or tubes, rather than the traditional spherical MNP.
2. While MNPs are constricted by the superparamagnetic limit to dimensions of a few nanometers, the dimensions of the MNS can be ranged from a few tens to thousands of nanometers.
3. As MNSs can be made of pure magnetic materials, they can show larger magnetic moments than MNPs. For their applicability in diagnosis, a large magnetic moment is highly recommended in order to enhance the sensor detection limit.
4. MNSs have been suggested for magnetomechanical action to induce cell damage at low frequencies and small external applied magnetic fields, which is not possible with MNPs. This scenario opens new possibilities in cancer therapies, since the technical requirements for the design of clinical equipment are much less challenging in this case than for the hyperthermia approach that needs high frequencies and strong magnetic fields, and has triggered the scientific interest of MNSs with unique spin configurations suitable for biomedical applications.[36–38]

In this review, we report the recent advances in nanotechnology and explored the value of emerging MNSs for biomedical applications, such as in cell manipulation and separation, MRI[30,39–43] and, in particular, for magnetomechanically induced cellular annihilation.[34,37,44] We will review the fundamental research made in this field from the synthesis of the MNS to the demonstration of the relevance of these nanostructures. First, this review will report the groundwork made in the fabrication of several types of magnetic nanostructures: micro/nanodisks in the spin-vortex state, synthetic antiferromagnetic structures (SAF-IP and SAF-OoP), and nanowires with high torque. Then, the revision of the biomedical approach will be focused on the physical properties of these nanostructures and their influence on the reported therapeutic efficacy.

II. VORTEX-STATE IN NANODISCS

New exotic magnetic configurations have been shown up at the nanoscale due to the interplay between different energy terms such as the dipolar, the exchange, and the anisotropy energy contributions. One of the most popular examples is the magnetic vortex configuration that has been shown as the ground state in ferromagnetic dots with different geometries (circular, elliptical, or triangular). In micro/nanodisks, the minimization of energy forces the spins into a curling state, where the spin directions change gradually, starting parallel to the surface, canceling the total dipole energy, and also not losing too much exchange energy. Near the center of the disk, the angles between adjacent spins increase until it is no longer possible to remain confined in-plane, resulting in a vortex core, with magnetization perpendicular to the plane,[45] as is illustrated in Fig. 1. Vortices are characterized by two features: (1°) The chirality that is related to the directions of the in-plane rotating magnetization (counterclockwise or clockwise); (2°) the direction of the vortex core's magnetization or polarity (up or down).

The vortex-type remanent magnetization distribution is energetically favorable for the disks with weak magnetocrystalline anisotropy[46] and is either deduced from the hysteresis loop's shape[47] or directly observed by magnetic imaging techniques like magnetic force microscopy (MFM).[48] Magnetic force microscopy (MFM) experiments in soft magnetic materials must be, however, interpreted carefully since unavoidable tip-induced perturbations must be taken into account.[49]

Figure 2 shows the magnetization dependence on the applied magnetic field. The loop was measured using a magneto-optical technique for the Permalloy (Py) disk array with a thickness of 60 nm and a diameter of 0.2 μm.[46] Decreasing the externally applied field leads to the nucleation of the vortex state, being accompanied by an abrupt decrease in magnetization. The field at which this phenomenon occurs is designated as the nucleation field, H_n. Then, a region where the magnetization responds linearly to the field follows, corresponding to the reversible movement of the vortex core, and includes the remanent state with virtually no magnetization, which can be seen in Fig. 2(a). As the individual moments tend to align with the field, this increasingly pushes the core to move perpendicularly to the direction of the field [Figs. 2(b) and 2(c)]. The continuous decrease in the field causes the vortex core to be expelled from the disk, marking the vortex annihilation field, H_a, after which the disk stabilizes in a single-domain state. The values of characteristic fields and the slope of the linear part of the hysteresis loop are strongly size dependent.[46,50–52] The direction of the magnetization at the center of the disk seems to turn randomly, either up or down, as up- and down-magnetizations are energetically equivalent without an externally applied field and do not depend on

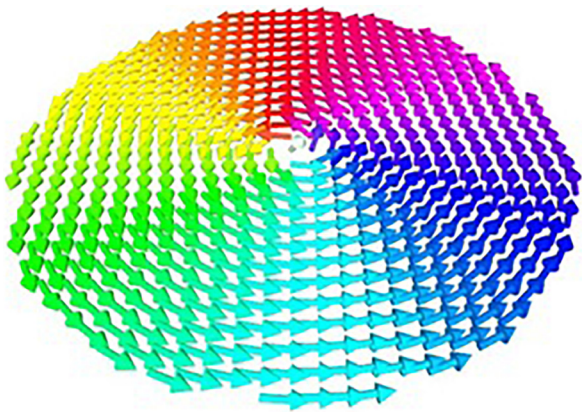

FIG. 1. Vortex core schematic.

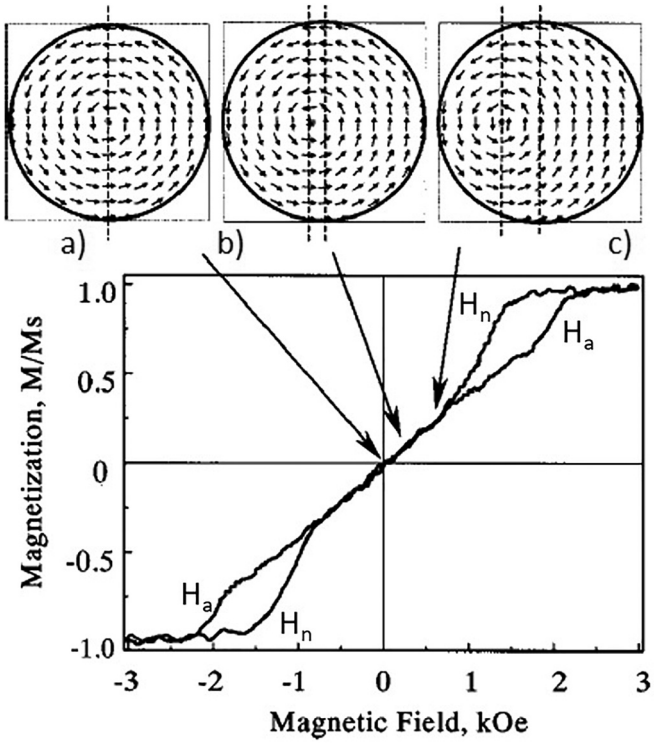

FIG. 2. Hysteresis loop that shows the vortex state.[46] Reproduced with permission from Guslienko *et al.*, "Field evolution of magnetic vortex state in ferromagnetic disks," Appl. Phys. Lett. **78**, 3848–3850 (2001). Copyright 2001 American Institute of Physics.

the vortex orientation. In summary, the magnetization reversal occurs starting with vortex nucleation followed by displacement and then annihilation of the magnetic vortex.

With negligible interdot coupling in the arrays, the magnetization reversal is initiated in accordance with the balance of the magnetostatic, exchange, and magnetic anisotropy energies. However, the magnetostatic interaction is important to describe the magnetic state of the patterned film, when the dot spacing is small. Arrays of magnetic structures whose geometry, size, and spacing can be controlled in the fabrication process are an appropriate term for comparison with theoretical predictions. The dot shapes are also an important factor for coupling calculations in such close-packed dot arrays.[50]

Permalloy (80% Nickel and 20% Iron alloy; Py) disks have been extensively studied, being capable of bearing this spin structure, within a finite range of dimensions. Other materials that have also been studied include Supermalloy (75% Nickel, 20% Iron, and 5% Molybdenum alloy), Cobalt, Nickel, and Iron. The main reports found in the literature are summarized in Table I, where the materials, deposition, and patterning techniques are shown.

A. Magnetization reversal in arrays of disks vs isolated disks

1. Aspect ratio

The material, the geometry, and mainly the aspect ratio of the structure are the key factors for achieving a vortex spin configuration as the ground state. Form the calculation of the single-domain and the vortex state energies, a universal magnetic phase diagram, as a function of dimensions, was determined for circular soft magnetic dots and in the absence of an external magnetic field (Fig. 3). The phase diagram shows the stability of the ground state as a function of the dot radius (R), dot thickness (L), and the material exchange length (LE).[53–56] The aspect ratio of the nanostructures is going to be the determinant to the spin configuration present in remanence, and so it is vital to understand which range of dimensions give us the vortex state. With this objective, a lot of work has been reported, where the magnetic behavior of arrays of disks with different diameters and thickness was extensively studied. Cowburn *et al.*[47] combined electron beam evaporation and electron beam lithography to fabricate various arrays of Supermalloy disks with diameters ranging from 55 to 500 nm and thicknesses between 6 and 15 nm. The results are summarized in Fig. 4, where different hysteresis loops for different dimensions are presented. Some of the loops do not show vortex behavior, which allowed the authors to experimentally determine a lower limit to the boundary for the transition from vortex to single-domain behavior, below which vortex nucleation is impossible.[47]

In 2000, Schneider *et al.*[52] studied the magnetic properties of circular Permalloy disks with the diameter ranging from 180 to 950 nm and a constant thickness (15 nm). It was observed that H_a strongly depends on the disk diameter, which was explained by the increasing contribution of the magnetostatic self-energy with the decreasing diameter, whereas H_n is almost constant (Fig. 5). Two years later, Schneider *et al.*[48] developed the same type of study for Permalloy cylinders with thicknesses of 3, 5.5, 8.3, 15, and 20 nm and diameters varying between 150 and 1000 nm. The characteristic vortex fields' dependence on the aspect ratio ($r = D/t$, where D is the diameter and t the thickness) was the main subject of this work. Then, the authors found that the absolute values of both H_a and H_n decrease with an increase in the aspect ratio ($r = D/t$). This behavior means that the single domain and intermediary states, which precede the formation of a vortex configuration, are more stable at large aspect ratio values. Moreover, it was also observed that the core of the vortex is not well centered in the thinnest disks ($t = 5.5$ nm). As it is slightly displaced, the remanent magnetization is nonzero. The authors suggested that this behavior could be understood assuming that the vortex can be pinned at positions where the energy has a local minimum and due to surface roughness.

On the other hand, Fernandez *et al.*[62] studied the magnetization reversal in Co elliptical dots varying the thickness from 18 to 30 nm by means of MFM. They highlighted the role of the shape anisotropy term in the domain configuration when the dots are not circular. In particular, a uniformly magnetized state was observed at remanence when the elliptical dots were saturated along their long axis. However, when dots were saturated along their short axis, they relax in a single-vortex state. It was suggested that this behavior could be associated with the film microstructure allowing the shape anisotropy to dominate over magnetocrystalline anisotropy contribution.

In summary, it has been experimentally confirmed that the values of characteristic fields (H_a and H_n), as well as the slope of the linear part of the hysteresis loop, are strongly material and size dependent.[46,50,51] Regarding the vortex core, the direction of the magnetization at the center of the disk seems to turn randomly, either up or down, as up- and down-magnetizations are energetically

TABLE I. Fabrication characteristics of the micro/nanodisks in the vortex state reported in the literature.

References	Material	Deposition technique	Patterning
34	Py ($t = 60$ nm, $D = 1000$ nm)	Magnetron sputtering	OL (Optical Lithography)
46	Py ($t = 60$ nm, $D = 200 - 800$ nm)	[a]	EBL (Electron-Beam Lithography)
35	Au (5 nm)/Py (60 nm)/ Au (5 nm); $D = 2\mu$ m	Thermal evaporation	ma-N 1410 resist As a milling mask
57	Au (5 nm)/Py (60 nm)/ Au (5 nm); $D = 1; 1, 5; 2; 2, 5\mu$ m	Magnetron sputtering	OL
47	Supermalloy ($D = 55 - 500$ nm; $t = 6 - 15$ nm)/Au (5 nm)	Electron beam evaporation	High-resolution EBL
45	Py ($t = 50$ nm, $D = 0, 1 - 1\mu$ m)	Electron beam evaporation	EBL
48	$D = 150 - 1000$ nm, $t = 3; 5.5; 8.3; 15; 20$ nm	Thermal evaporation	EBL
58	Fe ($t = 8$ to 9 nm); lateral dimensions of 200 to 500 nm by 150 to 250 nm	Evaporation	Self-organized Growth of Fe
59	Cobalt/Al_2O_3/Py ($t = 0 - 30$/ $3/0 - 30$;$D = 300$ nm)	RF sputtering	EBL
60	Co ($15 - 40$ nm)/Au (6 nm); Minor axis $= 250 - 375$ nm, Major axis $= 400 - 600$ nm	Thermal evaporation	IL (Interference Lithography)
50	Py ($t = 80$ nm; $D = 0, 2 - 0, 4\mu$ m)	Electron beam evaporation	EBL
51	Py ($t = 40$ nm; $D = 500$ nm)	Electron-beam evaporator	EBL
61	Py ($t = 5 - 50$ nm; $D = 0, 8\mu$ m)	dc magnetron sputtering	photolithography
62	Co ($t = 18 - 30$ nm; Minor axis $= 250$ nm, Major axis $= 450$ nm)	Thermal evaporation	IL
63	Fe ($t = 20$ nm; $D = 2\mu$ m)	Molecular beam epitaxy	EBL
64	Ni ($t = 16 \pm 1.5$ nm; $D = 40 - 90$ nm)	Electrodeposition	X-ray IL
65	Py ($t = 25$ nm; $D = 700$ nm)	[a]	EBL

[a]No deposition technique mentioned.

equivalent without an externally applied field and do not depend on the vortex orientation.

However, Waeyenberge *et al.*[66] demonstrated the switching of the out-of-plane core polarization by applying short pulses of a sinusoidal excitation field.

2. Effects of the interdot distance

Until this point, the magnetic behavior of isolated dots with a vortex configuration has been described. However, different behaviors have been observed in arrays of nanoelements, due to the magnetostatic coupling between them. Therefore, and assuming that several nanostructures would be required for any biomedical application, the effect of the interdot distance, d, is also an important factor that should be understood. Then, few of the more significant examples are briefly described next.

Experimental data and calculations reported by Novosad *et al.*[50] show a strong dependence of the vortex characteristic fields on the interdot distance. This is illustrated in Fig. 6, where are represented two hysteresis loops for arrays of disks with different distances between dots. The loops share the same shape, as expected for vortex-like behavior but have different H_n and H_a values. These values, as well as the slope of the linear part of the hysteresis loop, seem to depend not only on the dot diameter and the thickness but also on the interdot distance. It should be noted that H_n and H_a decrease, whereas an initial susceptibility of the vortex increases with the decreasing distance. The higher initial susceptibility means that the dot arrays with a strong interdot magnetostatic coupling ($d < D/2$) have a higher mobility of the vortex core than an isolated dot with the same size. The decrease in the values for the characteristic fields may be explained by the higher effective field experienced by each individual disk, from the contributions of the neighboring disks.[50]

Mejía-López *et al.*[67] studied the role of the magnetic interactions between Fe nanodiscs, with D = 65 nm and t = 20 nm, as a function of the center-to-center dot distance (d). Figure 7 shows the evolution of

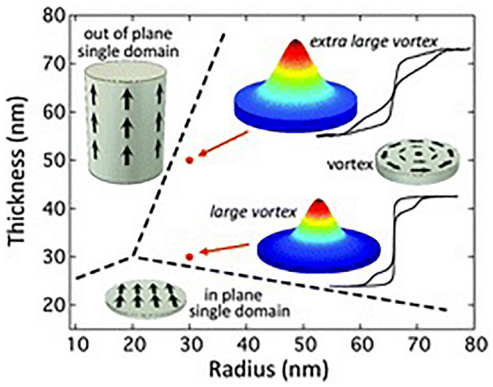

FIG. 3. Magnetic phase diagram of cylindrical dots with radius R and thickness L. Three stable magnetization states: vortex, in-plane single domain (small thickness), and perpendicular single domain (small radii). LE is the exchange length (LE 18 nm for Permalloy).[54] Reprinted with permission from Goiriena-Goikoetxea *et al.*, "Magnetization reversal in circular vortex dots of small radius," Nanoscale **9**, 11269–11278 (2017). Copyright 2017 Royal Society of Chemistry.

the characteristic vortex fields as a function of the normalized distance (d/D). The closer the dots are, the larger the absolute value of the vortex nucleation field is. It was suggested that when dots are mainly magnetized along one direction, the magnetostatic interaction favors such a configuration. Hence, an additional energy barrier for the transition from a single domain to the vortex state is created, which increases the vortex nucleation field values. On the other hand, the annihilation field is also affected by the interdot interaction, but this effect is less remarkable as the dipolar interactions between dots in the vortex state are weaker. In this work, it was stated that a dot array and a single dot show the same hysteresis loops when $d \geq 3D$. Also, the shape of the hysteresis loop is very similar to the noninteracting case for $2D \leq d < 3D$. Thus, it was concluded that the magnetic properties of two interacting dots can be well described by the behavior of noninteracting dots when $d \geq 2D$. On the other hand, the interaction between two magnetic dots is important and can significantly modify magnetization reversal when $d \leq 2D$.

The difference between simulated and experimental data was attributed to the distribution of dot sizes and imperfections of the shape of the dots in the experimental system. Also, the neglected interdot interactions, while not producing qualitative changes to the overall hysteresis loop shape, may contribute to some small quantitative corrections.[67]

Guslienko *et al.*[68] also observed that the magnetostatic interactions play an important role in the magnetization reversal for the disk arrays when the interdot distance is smaller than the disk radius. They developed an analytical model for the magnetization reversal process of a chain of interacting circular dots [in Figs. 8(a) and 8(b)]. Decreasing the field leads to vortex nucleation being initiated in two dots located at the ends of the chain, as they are neighbor free on one side and consequently under a smaller effective magnetic field than the more central dots. Once the disks at the edge nucleate a vortex state, their nearest neighbor disks are subsequently exposed to a reduced effective field, and the nearest neighbor disks can more easily nucleate a vortex.[68] The same conclusion was reached by Zhu *et al.*[51] when they observed, using MFM, that vortex nucleation initiates at the edge

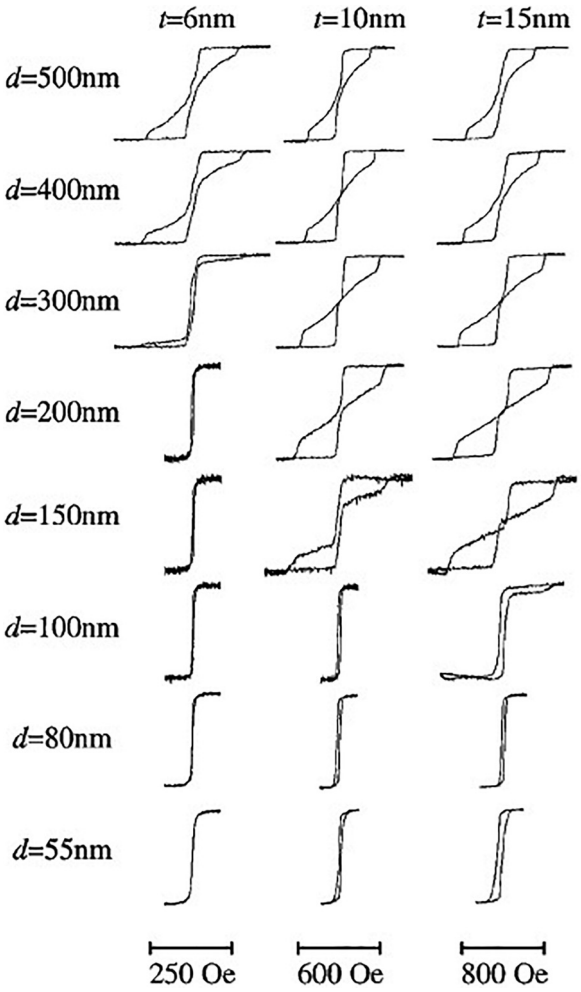

FIG. 4. Hysteresis loops measured as a function of diameter (*D*) and thickness (*t*), for Permalloy disks.[47] Reprinted with permission from Cowburn *et al.*, "Single-domain circular nanomagnets," Phys. Rev. Lett., **83**, 1042–1045 (1999). Copyright 1999 American Physical Society.

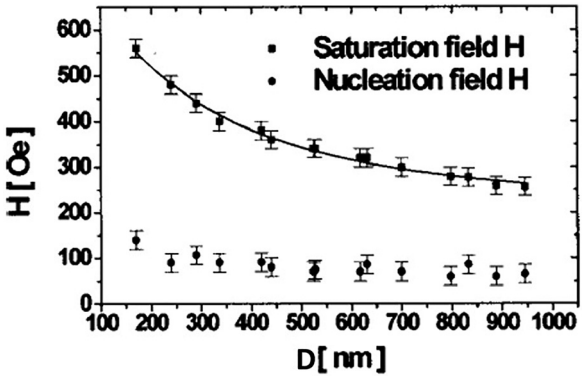

FIG. 5. Values of saturation and nucleation field vs diameter.[52] Reproduced with permission from Schneider *et al.*, "Lorentz microscopy of circular ferromagnetic permalloy nanodisks," Appl. Phys. Lett. **77**, 2909 (2000). Copyright 2000 American Institute of Physics.

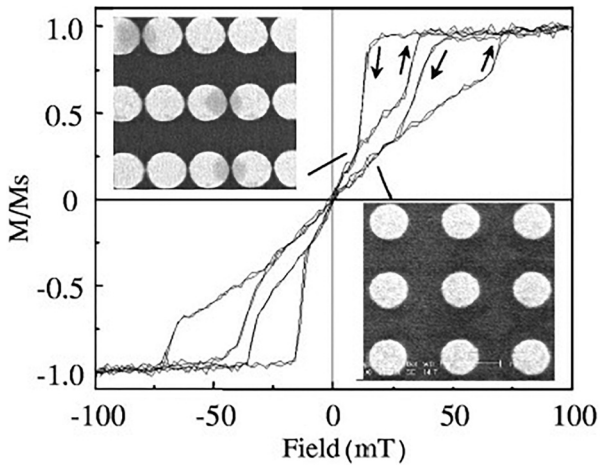

FIG. 6. Hysteresis loop Permalloy $D = 0.8\,\mu$m for different interdot distances, d, of 800 and 30 nm.[50] Reprinted with permission from Novosad *et al.*, "Effect of interdot magnetostatic interaction on magnetization reversal in circular dot arrays," Phys. Rev. B, **65**, 060402 (2002). Copyright 2002 American Physical Society.

of the chain, where dots have fewer neighbors, while the annihilation process occurs at the center of the chain.

More complex behaviors have been reported in the literature. Among them, we would like to briefly comment on the work of Heyderman *et al.*,[64] in which the distance between dots and their arrangement in the array can lead to the collective rotation of the magnetic spins. The authors considered that, rather than forming a vortex in each individual dot, the flux closure can occur through a series of dots to minimize the magnetostatic energy. Also, Neal *et al.*[63] studied the magnetization reversal in 2 μm diameter epitaxial Fe (1 0 0) disks using scanning Hall probe microscopy, supporting its findings with micromagnetic simulations. In this work, the simulations predicted the presence of a double vortex magnetization reversal process. Comparison between the magnetic images and local induction

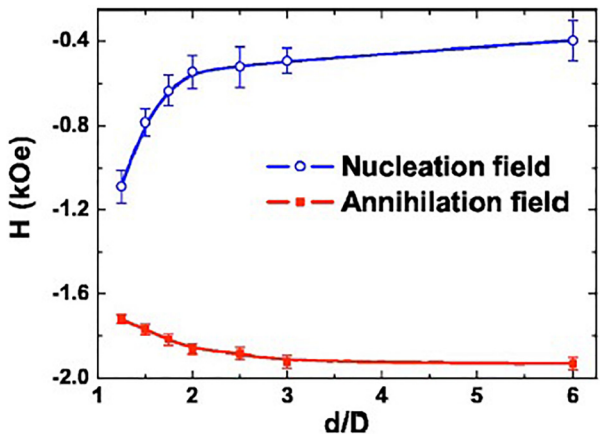

FIG. 7. Vortex nucleation and annihilation fields calculated as a function of d/D.[67] Reproduced with permission from "Vortex state and effect of anisotropy in sub-100-nm magnetic nanodots," J. Mejía-López *et al.*, J. Appl. Phys. **100**, 104319 (2006). Copyright 2006 American Institute of Physics.

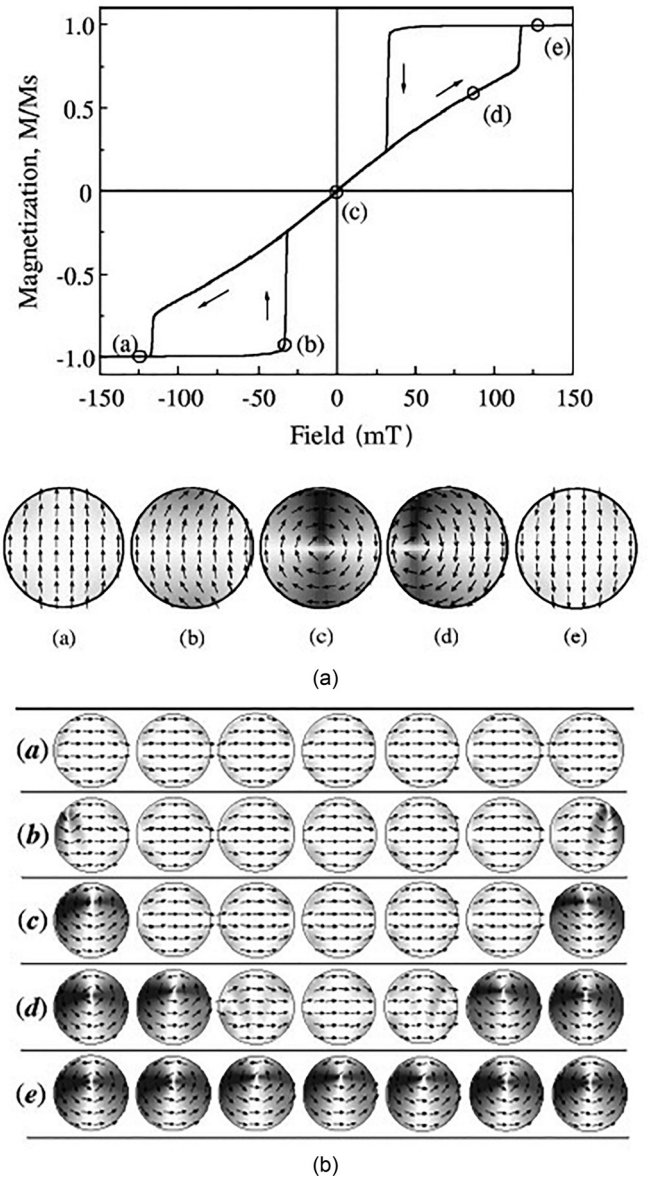

FIG. 8. Simulated data of a chain of seven dots with $R = 0.2\,\mu$m, $t = 60$ nm, and $d = 50$ nm.[68] Reprinted with permission from Guslienko *et al.*, "Magnetization reversal due to vortex nucleation, displacement, and annihilation in submicron ferromagnetic dot arrays," Phys. Rev. B, **65**, 244141–2441410 (2002). Copyright 2002 American Physical Society. (a) Hysteresis loop and (b) evolution of the spin structure in the chain of circular dots for different fields.

loops at strategic points on the disk shows that they seemed to agree well with this double vortex magnetization reversal mechanism.

III. SYNTHETIC ANTIFERROMAGNETIC NANOSTRUCTURES (SAF-IP AND SAF-OoP)

For biological applications, the desire to produce magnetic nanostructures with large moments and small, low-field, susceptibilities increased interest around Synthetic Antiferromagnetic (SAF)

particles.[30,69–71] These nanostructures are characterized by having two ferromagnetic layers separated by the one that is nonmagnetic. The coupling between the two ferromagnetic layers can be of two forms: magnetostatic or interlayer exchange coupling. While the magnetostatic interaction depends on the aspect ratio of the structure,[72,73] the indirect exchange coupling, through the Ruderman–Kittel–Kasuya–Yosida (RKKY) interaction, depends on the material and the number of interfaces and shows an oscillatory dependence between a ferromagnetic and an antiferromagnetic coupling as a function of the spacer thickness.[74–77] Therefore, the interlayer exchange coupling in SAF can be easily tailored by playing with the aspect ratio of the structure and/or the spacer between the magnetic layers, and they have been already applied for different devices such as in recording media[79–81] and magnetoresistive random access memory (MRAM) components.[82,83]

The antiferromagnetic behavior of these nanostructures means that, at low fields, the two ferromagnetic layers have antiparallel magnetizations, which then results in the near-zero remanence (see the diagram in Fig. 9). SAF systems, where the ferromagnetic layers show in-plane (SAF-IP) or out-of-plane magnetizations (SAF-OoP), have been reported, and few examples will be described in this section.

In 2008, Hu *et al.*[72] prepared 120 nm diameter SAF-IP disks, using Ru as the nonmagnetic spacer and $Co_{90}Fe_{10}$ as the ferromagnetic material, and it was demonstrated that its related magnetic properties can be tuned by exploiting the interlayer magnetic interactions.

The authors state that the effect of the indirect exchange coupling is weak when the thickness of the nonmagnetic spacer is above 2.5 nm. Then, the ferromagnetic layers primarily interact through magnetostatic interactions. Figure 10 shows the in-plane hysteresis loops of SAF-IP with the nonmagnetic and magnetic layer thicknesses of 2.5 and 12 nm, respectively. The remanence and coercivity of the nanoparticles are nearly zero as the magnetizations of the individual layers are antiparallel at low fields. As the external field is gradually increased, the moments of the individual ferromagnetic layers suffer an in-plane rotation toward the direction of the applied field until they are in a parallel configuration at the saturation field following a nearly linear field dependence of the magnetization.

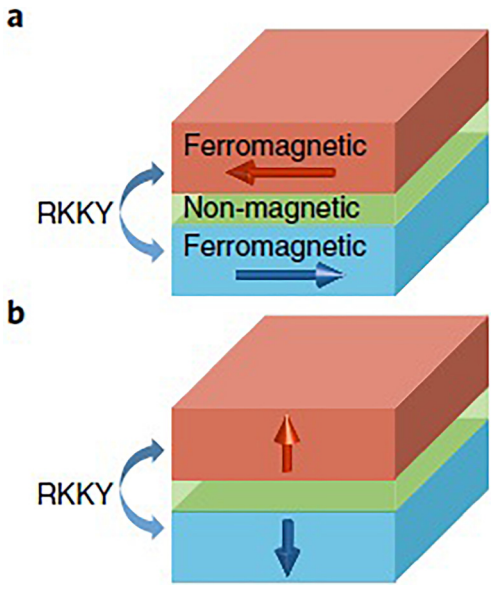

FIG. 9. Schematic of synthetic antiferromagnets. (a) Bilayers with in-plane magnetization. (b) Bilayers with out-of-plane magnetizations.[78] Reprinted with permission from R. A. Duine *et al.*, "Synthetic antiferromagnetic spintronics," Nat. Phys. **14**, 217–219 (2018). Copyright 2018 Springer Nature.

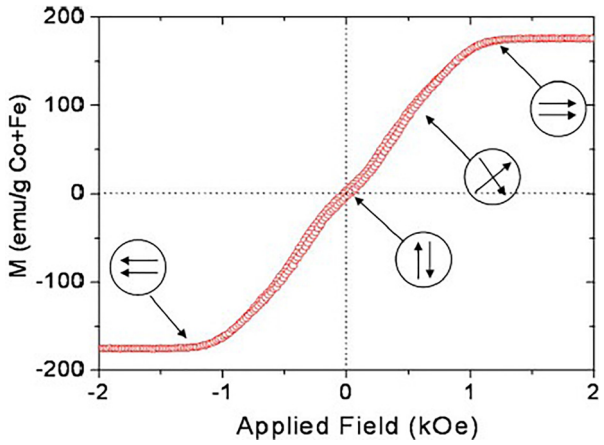

FIG. 10. Magnetic properties of 120 nm SAF nanostructures of Ta (5 nm)/Ru (2 nm)/$Co_{90}Fe_{10}$ (12 nm)/Ru (2.5 nm)/$Co_{90}Fe_{10}$ (12 nm)/Ru (2 nm)/Ta (5 nm), with the in-plane field perpendicular to the magnetic moments of the layers, from Ref. 73. Reproduced with permission from Hu *et al.*, "Synthetic antiferromagnetic nanoparticles with tunable susceptibilities," J. Appl. Phys. **105**, 07B508 (2009). Copyright 2009 American Institute of Physics.

Figure 11(a) shows the hysteresis loops of SAF-IP disks with the magnetic layer thickness ranging from 3 to 12 nm and the nonmagnetic layer thickness kept constant at 2.5 nm.[72] Again, both remanence and coercivity are nearly zero at low fields, but the saturation field and magnetization increase with the magnetic layer thickness (t_{mag}) because interlayer magnetostatic interactions increase linearly with t_{mag}.[84] This group also explored the effect of the indirect exchange coupling and observed that it is quite pronounced when the Ru spacer thickness is below 1 nm, which provides strong antiferromagnetic coupling.[72] Figure 11(b) shows the hysteresis loops of SAF-IP disks upon reducing the Ru spacer thickness from 2.5 to 0.6 nm while keeping the two CoFe layers at a thickness of 6 nm. The authors claimed that they were able to prepare SAF-IP nanoparticles with around 2.5 times higher saturation magnetization (850 emu/cm^3) than the iron oxide nanoparticles (340 emu/cm^3) usually used in biomedical applications.

More recently, Roosbroeck *et al.*[30] fabricated SAF-IP particles using Au as the nonmagnetic spacer and Permalloy as the ferromagnetic material and ranging the diameter from 90 to 525 nm (see the top panel of Fig. 12). They observed that the indirect exchange coupling oscillates between ferromagnetic (both layers are magnetized in the same direction) and antiferromagnetic (opposite direction) as a function of the spacer layer thickness. The saturation field oscillates between ferromagnetic (for Au thicknesses of 0, 1.5, and 3 nm) and antiferromagnetic (of 1 and 2.5 nm), see Fig. 12(a) in the bottom panel. Moreover, the oscillation is clearly damped with the increasing Au spacer thickness. Fig. 12(b) in the bottom panel shows two hysteresis loops using the spacer with the thickness for achieving ferromagnetic or antiferromagnetic couplings (1.5 and 2.5 nm, respectively). At

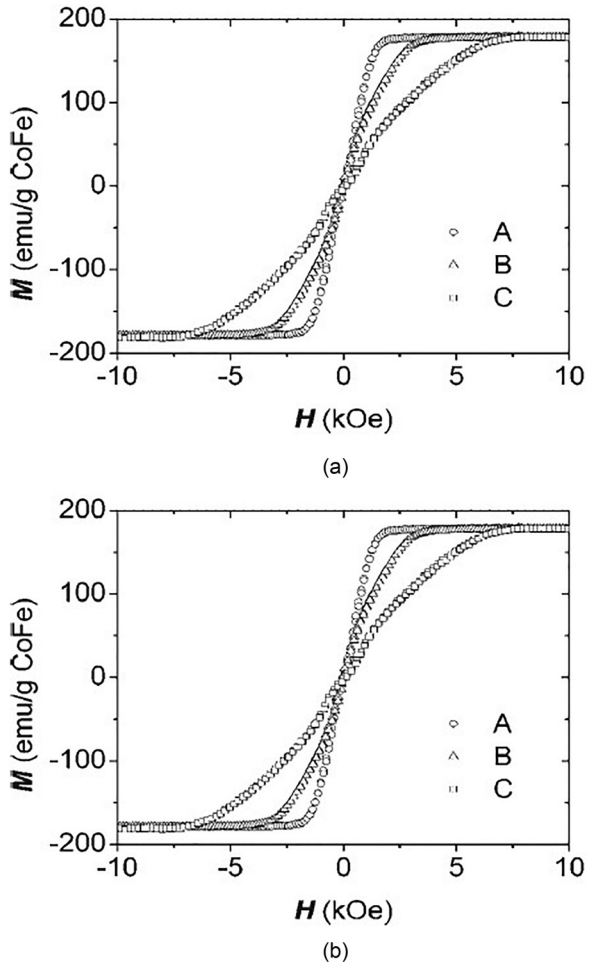

FIG. 11. Tailoring magnetic properties with magnetostatic and interfacial coupling, from Ref. 72. Hu *et al.*, "High-moment antiferromagnetic nanoparticles with tunable magnetic properties," Adv. Mater. **20**, 1479–1483 (2008).Copyright 2008 Wiley-VCH Verlag GmbH & Co. KGaA, Weinheim. (a) Hysteresis loops for different thicknesses of the magnetic layer. Circle, triangle, and square curves represent t = 3 nm, 6 nm, and 12 nm, respectively, and (b) Hysteresis loops for different thicknesses of the nonmagnetic spacer. Circles: Ta(5)/Ru(2)/CoFe(6)/Ru(2.5)/CoFe(6)/Ru(2)/Ta(5); triangles: Ta(5)/Ru(2)/CoFe(6)/Ru(0.6)/CoFe(6)/Ru(2)/Ta(5); and squares: Ta(5)/Ru(2)/[CoFe(3)/Ru(0.6)]3/CoFe(3)/Ru(2)/Ta(5).

1.5 nm, the loop corresponds to a standard ferromagnetic material with a high magnetic susceptibility. Increasing the thickness to 2.5 nm leads to lower magnetic susceptibilities and nearly zero magnetic remanence and coercivity, which is typical for antiferromagnetic coupling. For the SAF-IP, an average saturation magnetization of (4.15×10^5) A/m was determined, which is significantly higher than typical values for SPIONs used in MRI analysis $[(2.7–3.7) \times 10^5$ A/m$]$.[85]

Regarding the fabrication of SAF-OoP, one beautiful example is the work of Vemulkar *et al.*[71] in which perpendicularly magnetized (CoFeB/Pt) bilayers with antiferromagnetic interlayer coupling were fabricated. This structure consists of Ta(2 nm)/Pt(2 nm)/CoFeB(0.9 nm)/Pt(0.25 nm)/Ru(0.9 nm)/Pt(0.25 nm)/CoFeB(0.9 nm)/Pt(2 nm). The Ru spacer thickness was fixed to 0.9 nm because it corresponds to the first observed antiferromagnetic coupling peak.[77] The bilayer hysteresis loop, measured using a Magneto-Optical Kerr Effect (MOKE) magnetometer, showed an antiparallel state at low fields and an abrupt switch in the magnetization at a field, which can be controlled by tuning the interlayer exchange coupling between the magnetic layers via the Pt layer thickness.[86] Although the RKKY coupling should give an antiparallel state at a low magnetic field, with almost zero susceptibility, the authors suggested that the observed nonzero remanence can be attributed to the depth dependence of the MOKE signal. When a stack of 12 bilayers was studied, a field response comparable to the one of the single bilayer was observed without any degradation in the saturation magnetization or a significant change in the effective anisotropy of the layers.

Finally, the authors studied the possibility to transfer these properties to nanostructures with a diameter around 2 μm [Fig. 13(a)]. The MOKE hysteresis loop of a single 2 μm diameter SAF-OoP particle [Fig. 13(b)] is very similar to that of the nominally identical thin film. They showed that the perpendicularly magnetized SAF-OoP particles are characterized by zero remanence, low field susceptibility, and a distinct switching field to full magnetization. These particles show a precise tunability, making them ideal for tailoring to specific applications.

IV. HIGH ASPECT RATIO NANOSTRUCTURES

Higher aspect ratio nanostructures, such as nanowires (NWs) and nanorods, often appear as alternatives to the spherical magnetic nanoparticles, as this geometry translates into intrinsic anisotropy properties that cause them to interact differently.[87] They have an increased surface area to volume ratio and higher magnetic moments, originated from a prevalent shape anisotropy. Magnetic nanowires and their magnetic properties have long been a subject of intense study.[88–90] Segmented NWs have also been the topic of research due to their promising properties and applicabilities.[91–94] Several authors have already studied the interactions between the different layers on the same wire.[95,96] It has been theorized that for, infinite cylinders, the magnetization reversal mainly occurred in three different ways, Coherent rotation, magnetization curling, and magnetization buckling, and was found that the critical size for the single domain behavior was independent of magnetocrystalline anisotropy, depending only on the exchange constant and the saturation magnetization. The reversal mechanism chosen by the nanowire depends on the relation between the wire radius and the critical radius.[89]

The work of Wernsdorfer *et al.*[97] has shown, however, that the reversal process, in 40 to 100 nm Ni wires, results from the nucleation and propagation of a single magnetic domain along the wire. With this information, Ferré *et al.*[98] proposed that for real systems, even if with a weak crystal anisotropy was assumed, the reversal should be described in terms of nucleation-propagation mechanisms. In this work (see Fig. 14), these authors investigated the magnetic properties of electrodeposited Ni and Co nanowires with varying diameters (35–500 nm). It is revealed that intrinsic differences between the magnetization reversal mechanisms is originated from the difference in interplays between the magnetocrystalline and shape anisotropies. Ni's weak crystal anisotropy loses to the shape anisotropy of the wire, resulting in an easy axis parallel to the wire's axis, while Co's easy axis strongly depends on the magnetocrystalline anisotropy and the orientation of the hcp's c-axis. For larger diameters, the authors concluded that the c-axis was grown perpendicular to the wire axis, which

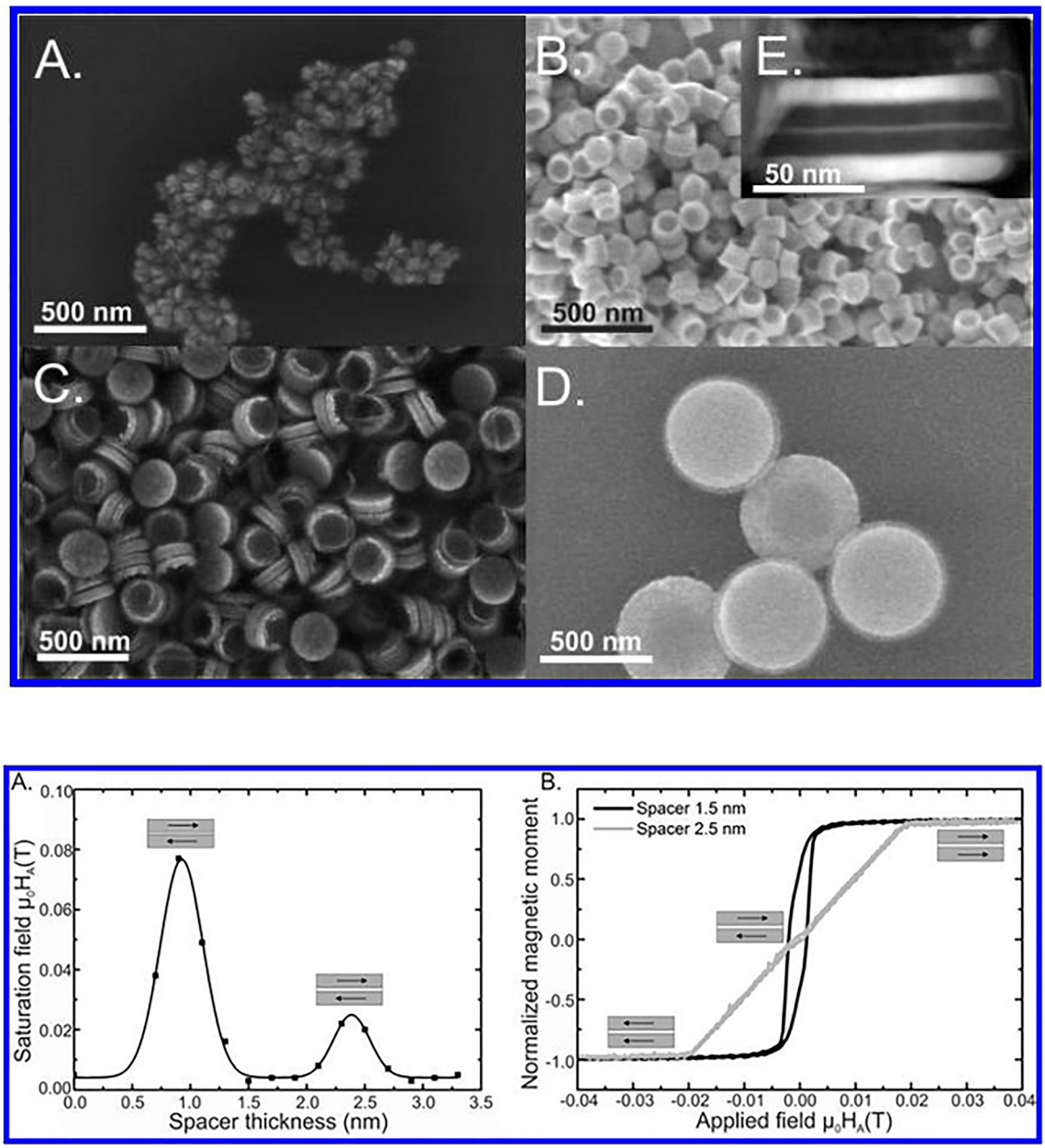

FIG. 12. Top panel: SEM images of SAF-IP nanoparticles with diameters of (a) 90, (b) 145, (c) 220, and (d) 525 nm. (e) High-angle Annular Dark-Field Scanning Transmission Electron Microscopy (HAADF-STEM) image of a 145 nm diameter SAF-IP. The layered structure of [Au/Ni80Fe20/Au/Ni80Fe20/Au] is clearly visible. The bright layers on top and bottom are the Au capping layers. The inner magnetic part consists of two Ni80Fe20layers (dark) separated by an Au spacer (bright). Bottom panel: (a) Magnetic saturation field of SAF-NPs in function of the spacer thickness. The trendline is a guide for the eye. (b) Magnetic hysteresis curves of 222 nm SAF-NPs [Au(10 nm)/Ni80Fe20(10 nm)/Au(xnm)/Ni80Fe20(10 nm)/Au(10 nm)], before release from the carrier wafer. The curves show a clear difference between ferromagnetic coupling (black, x = 1.5 nm) and antiferromagnetic coupling (gray, x = 2.5 nm). The schematic figures represent the magnetization directions of the magnetic layers in antiferromagnetically coupled structures at zero field and saturation field.[30] Reprinted with permission from Roosbroeck *et al.*, "Synthetic antiferromagnetic nanoparticles as potential contrast agents in MRI," ACS Nano **8**, 2269–2278 (2014). Copyright 2014 American Chemical Society.

explains the decrease in coercivity measured, due to the competition between the shape and crystal anisotropies, which is in agreement with the study by Proenca *et al.*[99] Moreover, these authors also showed, through micromagnetic simulations, that the reversal process, for small diameter Ni wires, is initiated by the nucleation of one reversed domain at one extremity, with its size being that of less than three times the exchange length, in diameter. For larger diameters, a different mechanism is described. The authors state the existence of

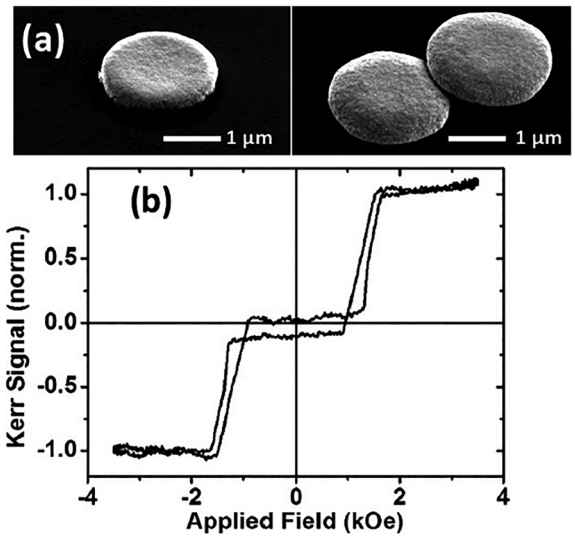

FIG. 13. (a) SEM images of 2 μm particles lifted off in solution and subsequently recondensed on a substrate. (b) Polar MOKE hysteresis loop of a single particle such as the one shown in (a).[71] Reproduced with permission from Vemulkar *et al.*, "Highly tunable perpendicularly magnetized synthetic antiferromagnets for biotechnology applications," Appl. Phys. Lett. **107**, 012403 (2015). Copyright 2015 American Institute of Physics.

two critical fields, the nucleation field (H_n), when the magnetization of the system deviates from the saturation, and the switching field (H_s), at which an irreversible magnetization jump occurs. In this scenario, the deviation from saturation takes place at the two extremities, resulting in propagating vortices along the wire. One possible explanation provided to us is that as it is the region where the coercivity field is at its lowest, the simulation not accounting for pinning defects or interactions between wires could be decisive. These simulations are in agreement with the study by Hertel,[100] who performed micromagnetic simulations in an array of closely packed Ni nanowires (l= 1 μm, d = 40 nm, and period= 100), and then Hertel and Kirschner[101] further investigated the magnetization reversal in Ni nanowires through micromagnetic simulations. In this work, the authors describe the basic reversal modes, transverse wall and vortex wall, with its occurrence depending on the thickness of the wire, even simulating a cone-shaped wire and observing the transition between the different reversal modes. The micromagnetic simulations in Co wires allowed the authors to affirm that for smaller diameters, the hcp c-axis's orientation differs from that of the larger ones.

Strijkers *et al.*[102] used nuclear magnetic resonance (NMR) to study the orientation of the c-axis of Co nanowires, with diameters of 20 nm and 100 nm. They found a switch over the easy-axis direction when the length of the wire was decreased from 40 μm to 0.5 μm. The longer wires were perpendicular to the wire easy axis, which would then change to be parallel to the wire axis, for the shorter ones. These authors also found that for a diameter of 100 nm, the Co wires presented an easy axis perpendicular to the wire axis, in contrast to the 20 nm diameter ones, which behaved more isotropic. In addition to this, Metzger *et al.*[103] deposited 770 nm long Fe nanowires and Co nanowires with a length of 64 nm and also found that the Co nanowires have a distribution of c-axis orientations.

Pignard *et al.*[104] studied Ni nanowires with a length of 22 μm and a diameter of 35 or 75 nm with Anisotropic magnetoresistance (AMR), which is caused by the changes in resistivity as the angle between the current and magnetization is modified. The AMR curves (Fig. 15) are composed of continuous variations of resistivity, corresponding to a rotation of the magnetizations, and discrete jumps in resistivity caused by magnetization reversal processes. These authors consider the reversal process starting with the nucleation of a reversed domain at the end of the wire, corresponding to the first discrete jump. The domain wall gets trapped in a pinning center, causing then the second jump when it is finally released, and the magnetization is reversed.

Nielsch *et al.*[105] studied the magnetic behavior of a periodic array of nickel nanowires with varying diameters, 30, 40, and 55 nm. In this work, it is stated that the magnetic anisotropy of the array results from the interplay of the different effective fields. For Ni nanowires compatible with the single domain, the weak magnetocrystalline anisotropy leads to an easy axis in the wire direction. These authors found that reducing the diameter from 55 to 30 nm improved the hardness and the coercivity, due to the lowering of the macroscopic interactions between the wires. The domain structure in Fig. 16 is reported to be due to an antiferromagnetic alignment, where two of its six nearest neighbors align their magnetization parallel and four are antiparallel, when only in accounting for the nearest interaction. Carignan *et al.*[106] also studied the influence of the diameter of Ni nanowires on their magnetic properties, with diameters of 20, 40, and 170 nm. The hysteresis loops for the three samples showed an easy axis parallel to the wire length, with decreasing coercivity and remanence for the increasing diameter, just as Nielsch *et al.*[105] The authors attributed the differences in the hysteresis loops to be caused by the different reversal processes. The 20 nm diameter wire is said to reverse magnetization through coherent rotation, while the one with a diameter of 170 nm does it through the curling mode and the 40 nm sample through transition between the two modes.

Pal *et al.*[107] studied the transition of the easy axis orientation in Co nanowires with respect to the aspect ratio (l/D) with both experimental values and micromagnetic simulations. These authors concluded that for larger aspect ratios ($R > 10$), shape anisotropy was the dominant contribution, which leads to an easy axis parallel to the wire. For aspect ratios shorter than $R < 3$, they stated that the magnetocrystalline anisotropy prevails and the easy axis is now orientated perpendicular to the wire axis, while for intermediary aspect ratios, the anisotropies are said to be comparable, resulting in difficult to distinguish differences between the axis. Several authors have studied different ways to influence the easy axis direction not only by changing the dimensions of the wire but also by changing its composition[108,109] and studying how it is affected by magnetoelastic anisotropy.[110]

Xiang *et al.*[111] performed micromagnetic simulations for individual Fe nanowires with different lengths and diameters to investigate their reversal mechanisms. In Fig. 17, different reversal mechanisms are showed to be in play, for different thicknesses. For the first two thicknesses [Figs. 17(a) and 17(b)], the mechanism identified by the authors is a coherent rotation. In Fig. 17(c), the reversal is associated with a vortexlike nucleation, initiated at the two ends of the nanowire. Regarding the last wire [Fig. 17(d)], the reversal mechanism is identified as being controlled by the buckling like motion of larger vortices, which also initiates reversal along the wire, instead of just the extremities.

Qin *et al.*[112] studied the magnetization reversal on Fe nanowires, being in agreement with the study by Xiang *et al.*,[111] but also focused

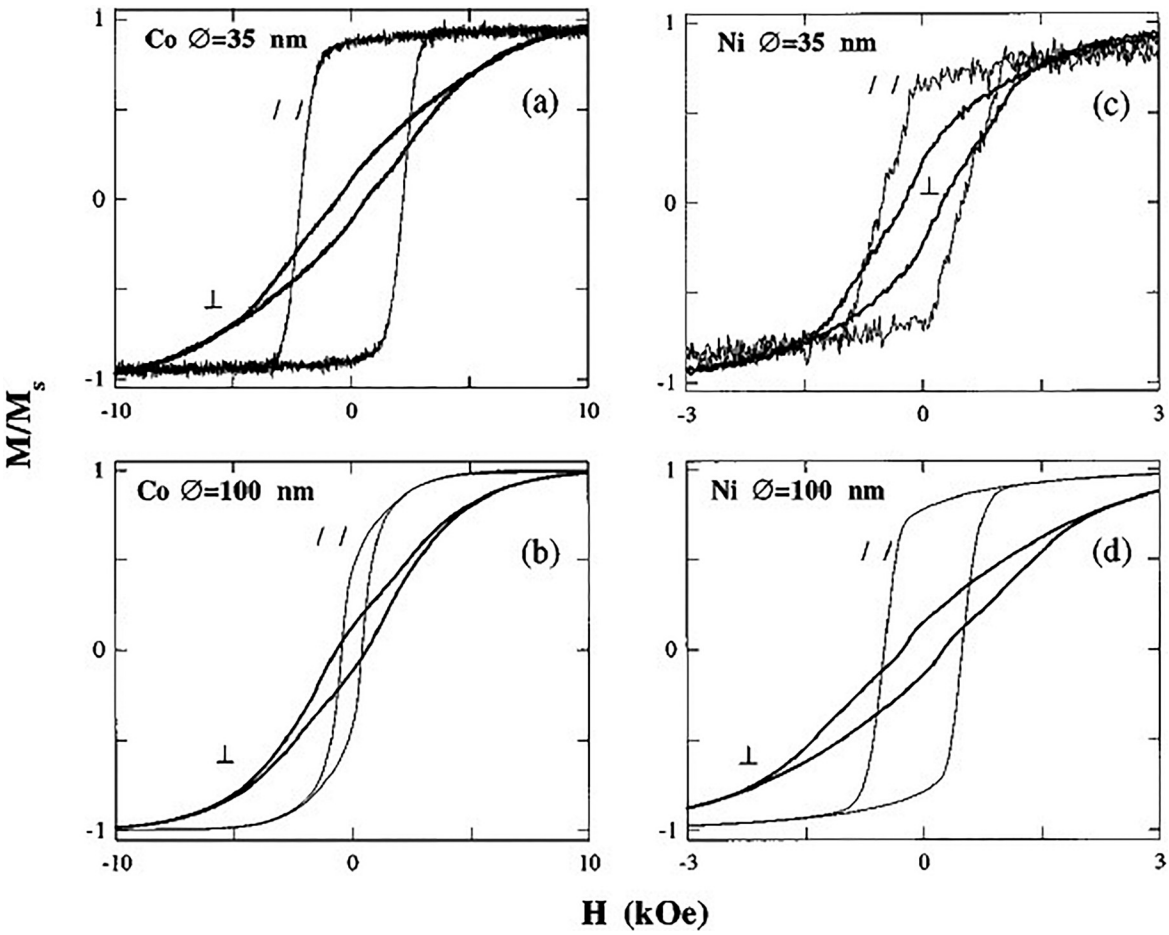

FIG. 14. Hysteresis loops for different thicknesses of Ni and Co.[98] Reprinted with permission from Ferré *et al.*, "Magnetization processes in nickel and cobalt electrodeposited nanowires," Phys. Rev. B, **56**, 14066–14075 (1997). Copyright 1997 American Physical Society.

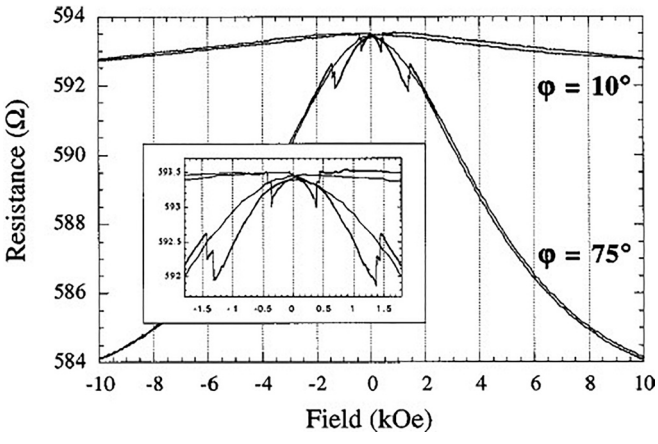

FIG. 15. AMR curves for Ni nanowires from the study by Pignard *et al.*[104] Reproduced with permission from Pignard *et al.*, "Study of the magnetization reversal in individual nickel nanowires," J. Appl. Phys. **87**, 824–829 (2000). Copyright 2000 American Institute of Physics.

on the effects of the magnetic interactions in a periodic array. The wire diameters were 30, 50, and 70 nm, and the interactions between the wires were found to be weakening the shape anisotropy effect, tending to develop an easy axis perpendicular to the wire's axis.

Ivanov *et al.*[113] provided an extensive record of micromagnetic simulations based on Py, Ni, Fe, and Co, varying the diameters from 20 to 100 nm, with a fixed length (20 μm). In this work, three main reversal modes are recognized as coherent rotation, where there is a homogeneous rotation of the magnetization along the wire, and transverse domain wall and vortex domain wall modes, where there are nucleation and propagation of a domain wall, transverse and vortex, respectively. The transition between the two domain wall modes is said to be expected to come with the increasing diameter, depending mainly on the material in question and its exchange length. These authors simulated hysteresis loops for individual wires and 7 coexisting wires and found that for all the materials, except Co, the easy axis did not really depend on the wire diameter and was parallel to the wire long axis. For all nanowires, the coercivity still decreased with the increasing diameter, due to the scaling of the shape anisotropy with the aspect ratio (l/D). For Co nanowires, it is stated that the orientation

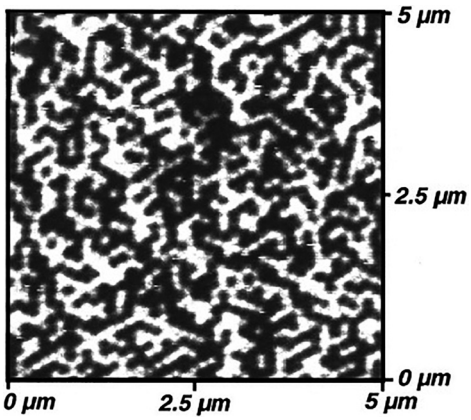

FIG. 16. MFM image of a periodic array of Ni nanowires in the demagnetized state.[105] Reproduced with permission from Nielsch *et al.*, "Hexagonally ordered 100 nm period nickel nanowire arrays," Appl. Phys. Lett. **79**, 1360–1362 (2001). Copyright 2001 American Institute of Physics.

of the magnetocrystalline anisotropy with respect to the wire axis will increase or decrease the effective anisotropy of the wires, leading the authors to believe that these properties can be tuned by controlling the crystal growth direction.

V. BIOMEDICAL APPLICATIONS

Among all nanomaterials applied in the biomedical field, magnetic nanostructures are one of the most frequently used, mainly due to their nontoxicity, biocompatibility, and inducible magnetic moment, which allows their remote control by the application of a magnetic field.[114,115] Consequently, there are multiple contexts where these magnetic nanostructures can be employed, such as cellular therapy involving cell labeling and targeting, as a tool to separate and purify cell populations, regenerative medicine, targeted drug delivery, contrast agents in magnetic resonance imaging (MRI), hyperthermia, or magnetomechanically induced cellular annihilation.[116,117]

Superparamagnetic nanoparticles (typically made of iron oxide) are undoubtedly one of the most widely studied and used nanomaterials in the biomedical area, particularly due to their zero remanence.[118,119] This is an important requirement for the biomedical application of nanostructures as it prevents them from agglomerating when dispersed in a solution.[38] Nevertheless, these nanoparticles have some drawbacks, such as low magnetic moment and reduced cargo capacity, which limit their efficiency.[38,120]

Therefore, this section addresses specific biomedical applications, namely, cell manipulation and separation, contrast enhancing agents in MRI, and magnetomechanically induced cell annihilation, where magnetic nanostructures, such as vortex or synthetic antiferromagnetic (SAF) nanodiscs and nanowires, can provide an improvement and/or surpass the limitations of the superparamagnetic nanoparticles.

A. Cell manipulation and separation

Efficient isolation and sorting of particular cells from heterogeneous populations are essential for various cell-based applications in multiple areas, such as cell and molecular biology, biochemistry, and

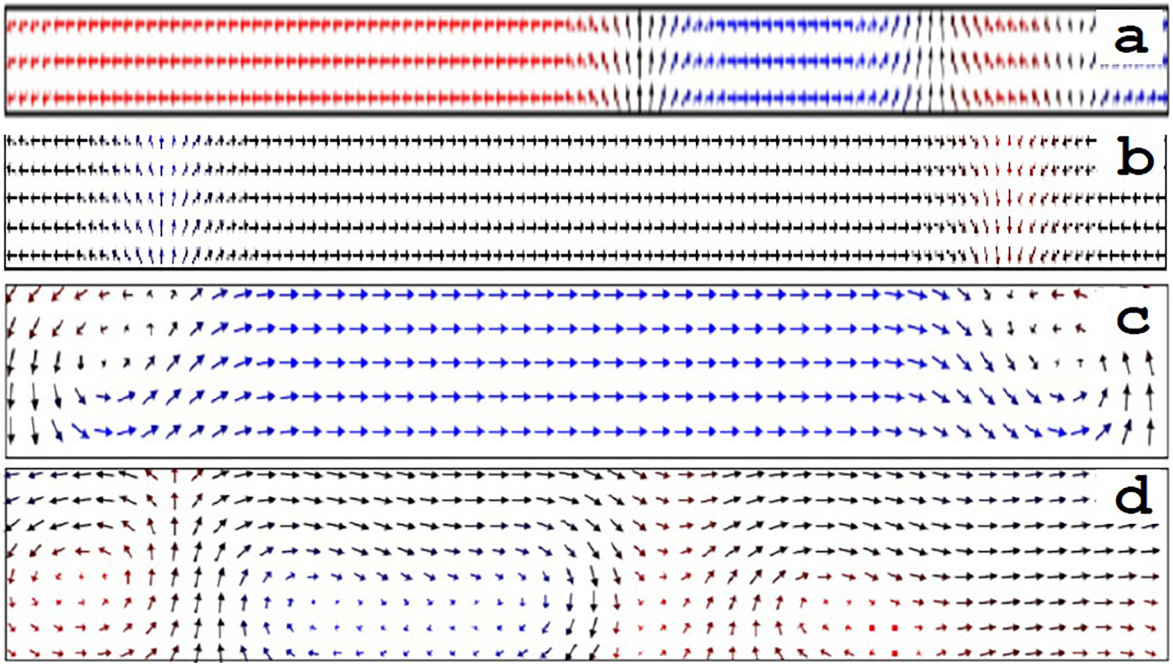

FIG. 17. Vector map of the spins when the reversal is triggered in Fe nanowires with l = 200 nm and d = 6 nm (a), 10 nm (b), 20 nm (c), 30 nm (d).[111] Reprinted with permission from H. Xiang *et al.*, "Micromagnetic simulations of magnetization reversal of iron nanowire," J. Phys.: Conf. Ser. **266**, 012022 (2011). Copyright 2011 IOP Publishing Limited (IOP) under the terms of the Creative Commons Attribution (CC BY) license.

immunology, as well as for clinical research.[121,122] Clinically, the detection and purification of specific cells are fundamental for the diagnosis, treatment, and prevention of diseases, being required, for example, in the acquisition of a particular population for transplantation and gene therapy or to separate the stem and progenitor cells for cancer treatment.[122,123]

Over the years, multiple cell isolation and manipulation techniques, based on physical characteristics, such as density or size, and on electric, magnetic, or adhesive properties of the cells, have been developed.[124] The standard processes for the separation of cellular populations include steps of filtration, density gradient centrifugation, and sedimentation.[124,125] However, when the different cells have similar sizes or densities, techniques based on those features cannot perform an effective separation.[126] Consequently, other methods, such as fluorescence-activated cell sorting (FACS) and magnetic-activated cell sorting (MACS), where magnetic nanostructures play a key role, must be used.[124,127]

A common approach involves coating superparamagnetic iron (Fe) oxide beads, i.e., a nonmagnetic matrix filled with superparamagnetic nanoparticles, with antibodies that are specific for the surface antigens of target cells.[125,128,129] In this methodology, the cells of interest, located in a heterogeneous cell population, are attached to the beads through antibody-antigen interactions and then separated by applying an external magnetic field.[122]

However, due to the reduced magnetic moments of the nanoparticles, this process frequently requires high external magnetic fields in order to efficiently isolate the target cells.[124] Therefore, such an approach could be enhanced if the superparamagnetic iron oxide beads were replaced by a nanoarchitecture with a higher magnetic moment. As a result, ferromagnetic nanowires and SAF nanostructures have been analyzed as potential candidates for the improvement of the current magnetic cell separation and manipulation techniques.

Ferromagnetic nanowires have been studied in this context due to their high aspect ratio, shape anisotropic properties (which lead to a single domain structure), large remanence, and high intrinsic magnetization, i.e., magnetic moment per unit volume.[122,130,131] Various reports, addressing the separation and manipulation of different cell lines using ferromagnetic nickel (Ni) nanowires functionalized with antibodies,[39,40,122,132,133] have demonstrated that these nanostructures perform better than the typical superparamagnetic beads of comparable volume, due to their higher saturation magnetization when compared to that of the beads (see Fig. 18).[39,40,122,132,133]

Nevertheless, it is crucial to assess the biocompatibility of these nanostructures, due to the potential toxic effects associated with some materials (for example, Ni).[134] Byrne *et al.*[135] studied the cellular response of a human monocytic cell line (THP-1) to Ni nanowires, having demonstrated that there were little or no toxic effects on the cells for short incubation periods (10 h) and at low concentrations (<100 nanowires per cell). Felix *et al.*[136] also addressed this topic, but on human fibroblasts (WI-38). In their work, it was verified that for incubation times shorter than 48h and low concentrations of nanowires (<11.88μg/ml), more than 80% of the cells remained viable; however, for longer periods, a significant decrease in their metabolic activity was observed. Furthermore, considerable toxic effects on the cells occurred mostly after 48 h and at high concentrations of nanowires (>22.5 μg/ml), with cell viability decreasing as the incubation time increased.

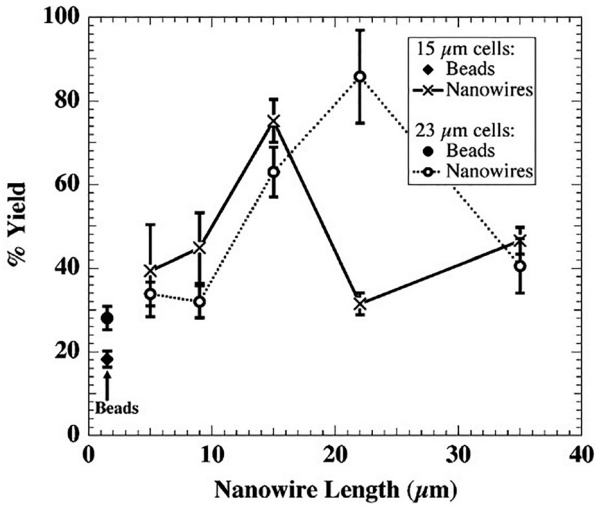

FIG. 18. Percentage of the initial number of cells with magnetic particles that were captured (% Yield), for beads and different lengths of nanowires, in the separation of mouse fibroblast (3T3) populations with average diameters of 15 μm and 23 μm.[39] Reprinted with permission from Hultgren *et al.*, "High-yield cell separations using magnetic nanowires," IEEE Trans. Magn. **40**, 2988–2990 (2004). Copyright 2004 IEEE.

As a result, it would be of interest to fabricate and characterize magnetic nanowires with similar physical properties, but constituted by more biocompatible materials. In this context, Ivanov *et al.*[130] fabricated and analyzed Fe nanowires as well as hybrid metallic/nonmetallic nanowires, composed of a Fe core and a Fe oxide (magnetite/Fe_3O_4) shell. The magnetic characterization performed showed that both kinds of nanostructures presented a single-domain magnetic state with a longitudinal magnetic anisotropy at remanence. Afterward, a cell viability test (Fig. 19), performed on colon carcinoma epithelial cells (HCT 116), indicated a high level of biocompatibility for these nanostructures. It was also proved that the coercive field, as well as the saturation and remanent magnetizations, can be tuned by varying both the core and the shell dimensions of the core-shell nanowire.

Additionally, Alsharif[137] and Alsharif *et al.*[138] studied the toxicity of functionalized Fe nanowires, with longitudinal magnetic anisotropy, in the recognition and binding to leukemic cells (HL60). In this case, the considered magnetic nanostructures (average diameter of 35 nm and around 3 μm length) were coated with bovine serum albumen (BSA) and (3-aminopropyl)triethoxysilane. Then, the BSA-coated nanowires were functionalized with a specific antibody (anti-CD44) that targets a surface marker (CD44) overexpressed on leukemic cells. After the incubation of the one-dimensional nanostructures with the cancer cells, a high level of *in vitro* biocompatibility for both coatings of the Fe nanowires and antibody-coated nanowires was observed.

Besides nanowires, SAF nanostructures have also been evaluated as possible surrogates to superparamagnetic beads in cell separation and manipulation applications. For example, by modifying the surface of SAF nanoarchitectures with a protein (streptavidin), Fu *et al.*[139] demonstrated that these nanostructures allow an improved detection of target biomolecules at low concentrations (10 ppm), when compared to the typical superparamagnetic materials.

Furthermore, by applying fluorescence labeling and adjusting the thickness of the magnetic layers, the authors could not only see the

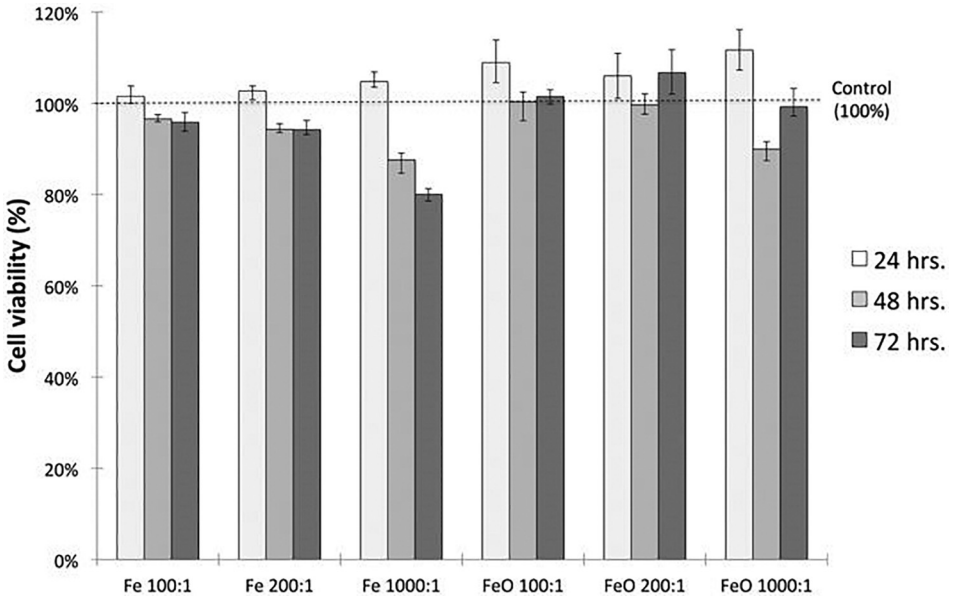

FIG. 19. Percentage of viable HCT 116 cells incubated with different concentrations of Fe and Fe-Fe_3O_4 core-shell nanowires for 24, 48, and 72 h. The concentrations on the x-axis indicate the nanowire-to-cell ratio.[130] Reprinted with permission from Ivanov *et al.*, "Tunable magnetic nanowires for biomedical and harsh environment applications" Sci. Rep. **6**, 24189 (2016); Copyright 2016 Authors licensed under a Creative Commons Attribution (CC BY 4.0) license.

motion of the SAFs in response to a small external magnetic field gradient ($10\,Tm^{-1}$) but also the dramatically modified movement, which can be very useful to separate and manipulate biological targets or materials linked to SAF surfaces through the application of magnetic fields. Therefore, from this report, it is possible to conclude that SAF nanostructures, due to their high magnetic moment per particle and multifunctional (optical, magnetic, and specific targeting) properties, provide a promising new path for multiple biomedical applications, such as biomolecule detection and magnetic manipulation.

An *in vitro* study on these particular nanostructures was performed by Zhang *et al.*,[41] where they were used to separate lung cancer cells (H1650) from blood samples. First, these particles were coated with a silica shell and then conjugated with streptavidin in order to be capable of linking to the cells of interest, making them highly magnetically responsive. Then, after the incubation of the cancer cells with the nanostructures, blood samples were mixed with the stained cells. Afterward, the spiked blood samples were pushed through a magnetic separation device (Fig. 20) and the captured cells were analyzed using an optical microscope. In this process, a capture efficiency of 46.8% was achieved, indicating that SAF nanostructures can indeed be used for the separation of cells from blood samples and, when combined with a subsequent optical analysis, possibly contribute to cancer detection in an initial stage.

B. Contrast agents in MRI

Magnetic Resonance Imaging (MRI) is a noninvasive imaging technique frequently performed all over the world.[43] A fundamental principle of MRI is the precession of nuclear magnetic moments when they are placed in an external magnetic field.[140] As a result of that motion, when a given sample, with several magnetic moments randomly oriented, is placed inside a strong magnetic field, a net magnetization in the direction of that field, called longitudinal magnetization, is generated.[141]

Through the application of a properly adjusted radio frequency (RF) pulse, it is possible to tip this magnetization out of alignment and originate a transverse magnetization component.[142] When the RF pulse is removed, both components of the magnetization will return, or "relax," to their previous states in the presence of a static magnetic field.[143] Therefore, due to this relaxation process, there is the production of a weak RF signal, which is detected by RF coils and subsequently processed in order to produce an image.[144]

The main advantages of MRI are the use of nonionizing radiation, high spatial resolution, great anatomic detail, and improved soft tissue contrast.[42,43] Such properties make this technique an appealing option to diagnose various physiological diseases and lesions, as well

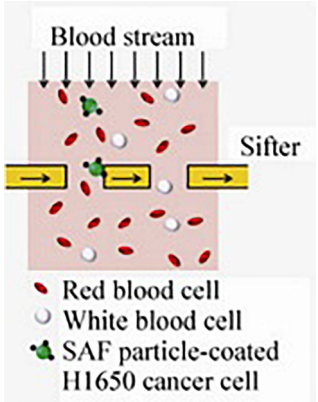

FIG. 20. Illustration of a blood sample, spiked with lung cancer cells, passing through the magnetic separation device (sifter); only cells linked to SAF nanostructures are captured by the sifter.[41] Reprinted with permission from Zhang *et al.*, "Functionalization of high-moment magnetic nanodisks for cell manipulation and separation," Nano Res. **6**, 745–751 (2013). Copyright 2013 Springer Nature Customer Service Center GmbH: Springer Nature.

as to assess the result of therapeutic treatments.[43] However, due to the very low sensitivity of MRI, contrast agents are often employed in order to increase the contrast of the acquired images and consequently facilitate the distinction between different tissues.[42,43]

MRI contrast agents enhance image quality by reducing the relaxation times of the nearby water protons and, consequently, changing the signal intensity of the water present in body tissues that contain the agent.[145–149] These contrast agents are commonly grouped in two classes, according to their predominant effect on relaxation rates:

1. T1 contrast agents: mainly shorten the relaxation time of the longitudinal component of the magnetization;[42,150,151]
2. T2 contrast agents: mainly shorten the relaxation time of the transverse component of the magnetization.[42,150,151]

The most widely used contrast agents in clinical practice are Gd^{3+}-complexes; however, these have raised various toxicity concerns.[152–156] Consequently, the interest for searching and studying new and safer alternatives has arisen. In this context, superparamagnetic iron oxide nanoparticles have been developed as viable alternatives to the Gd^{3+}-complexes. Such particles are typically used as T2 contrast agents, and they have various advantages, namely, biocompatibiliy, ability to be metabolized, relatively high saturation magnetic moments, and ease of surface functionalization.[42,43]

Nevertheless, the dimensions of such nanoparticles are restricted by the superparamagnetic limit, which implies a maximum diameter of 10–20 nm per particle in order to maintain zero remanence and consequently avoid their aggregation in the absence of a magnetic field.[157,158] As a result of this condition, the magnetic moment of each particle is limited and, unfortunately, the ideal particle size for MRI contrast agents, as determined by simulations, surpasses the superparamagnetic threshold.[159]

To overcome this difficulty, multiple approaches have been considered, such as increasing the magnetization of the nanoparticles within the superparamagnetic limit by using dopants or designing methods for controlled clustering of nanoparticles.[30,160] However, these approaches are tedious and produce clusters with sizes that are difficult to control.[30] Therefore, an alternative to these superparamagnetic nanoparticles would be to design nanostructures with larger magnetic moments that are not restricted by the superparamagnetic limit. In this context, several authors have studied various alternatives to the commercially available contrast agents.

For example, Bailey *et al.*[161] fabricated RE_2O_3-based nanodiscs (diameter ~10–14 nm), where RE = Gd, dysprosium (Dy), or ytterbium (Yb), passivated with a biocompatible polymer (Poly(acrylic acid)) (PAA) grafted with short methoxy-terminated polyethylene oxides), and analyzed their suitability as MRI contrast agents. The relaxation times of these nanostructures, measured at 37 °C (body temperature) in a magnetic field of 1.41 T, were compared against the reported values for their spherical counterparts or small molecule chelates, based on the commonly used pentetic acid (DTPA) ligand. The authors also performed a MRI of a phantom for all the considered contrast agents, using T1- and T2- weighted pulse sequences. The obtained results showed that Gd_2O_3 nanodiscs, in particular, present significant advantages over the commercially available Gd-DTPA contrast agents, namely, higher relaxivity, i.e., the change in the relaxation rate normalized to the concentration of the contrast agent, per particle.[162] This factor should increase the efficiency of *in vivo* targeted imaging schemes since it becomes possible to get a high amount of proton relaxation without requiring multiple small molecules in contact with the imaging target. Besides this benefit, it was verified that these Gd_2O_3 nanodiscs are suitable as both T1 and T2 contrast agents. Also, no significant cytotoxic effects were observed (Fig. 21), for the polymer coated Gd_2O_3 and Dy_2O_3 nanoarchitectures, on a human cell line derived from cervical cancer cells (HeLa).

On a different study, Singh *et al.*[163] fabricated and analyzed the suitability of polyethylene glycol (PEG)-coated Gd_2O_3 paramagnetic nanodiscs as well as PEG-coated Gd-doped iron oxide (GdIO) superparamagnetic cubic/spherical-shaped nanoparticles, with different dimensions, as MRI contrast agents. In this case, the relaxivities of the different nanoarchitectures were measured using a 7 T magnetic resonance (MR) scanner, and it was demonstrated that smaller sized

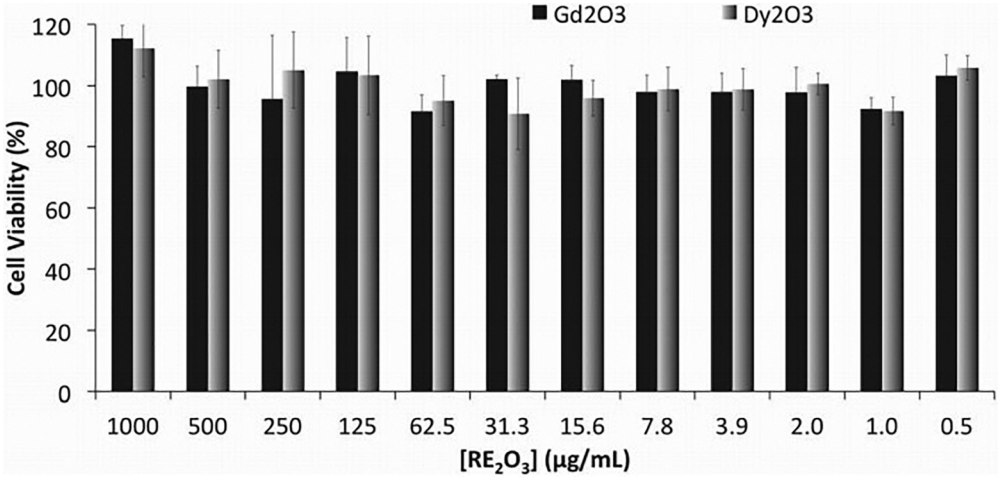

FIG. 21. Cell viability after a 48 h incubation with Gd_2O_3 and Dy_2O_3 nanodiscs passivated with a biocompatible polymer.[161] Reprinted with permission from Bailey *et al.*, "Stealth rare earth oxide nanodiscs for magnetic resonance imaging," Adv. Healthcare Mater. **1**, 437–442 (2012). Copyright 2012 WILEY-VCH Verlag GmbH and Co. KGaA, Weinheim.

nanostructures (<5 nm) resulted in effective T1 contrast agents; however, for larger dimensions (>5 nm), they became more suitable for reducing T2. Furthermore, no acute *in vitro* toxicity was found for the fabricated nanoarchitectures on glioblastoma-astrocytoma cells.

Besides nanodiscs, nanowires have also been addressed by some reports in the context of this biomedical application. Bañobre-López *et al.*[43] evaluated the relaxivity properties of polyacrylic acid (PAA)-coated Ni nanowires, with a longitudinal magnetic anisotropy, in a colloidally stable water dispersion. This dispersion was produced through a process of pulsed electrodeposition of Ni/Gold (Au) multilayer nanowires inside a porous alumina template in a three-electrode cell at room temperature, followed by the liberation of the Ni/Au multilayer nanowires from the template and then a two-step acidic etching. The relaxation times of these nanostructures, which presented a monodisperse average diameter and length of ∼36 nm and ∼600 nm, respectively, were measured using a relaxometer operated at 60 MHz and 37 °C for two magnetic fields, namely, 1.41 and 3 T. In both situations, the obtained results indicate that these nanostructures are efficient as T2 contrast agents. The contrast effect of the PAA-coated Ni nanowires was verified by performing a MRI of a phantom at a magnetic field of 3 T (Fig. 22).

Shore *et al.*[42] also studied nanowires in this context; however, they analyzed Fe and Fe-Au nanowires, fabricated by template-assisted electrodeposition with various lengths and diameters. These nanostructures were coated with compounds, namely, Dop-PEG and/or SH-PEG-COOH, which allow the binding of biological molecules to the nanowires in order to target specific cells. The magnetic characterization of both nanostructures indicated that the Fe-Au nanowires exhibit a larger saturation magnetization, due to the fact that their Fe layers are thinner than the diameter of the nanostructures, allowing them to be more easily magnetized in the direction perpendicular to the long axis of the nanoarchitecture, when compared to the Fe nanowires. The relaxivity properties of the nanowires were measured at 25 °C in a 1.5 T magnetic field and compared against Fe and Fe-Au nanoparticles. It was verified that the Fe nanowires with a length of 0.7 μm and a diameter of 110 nm, coated with Dop-PEG, were the best suited as T1 contrast agents. On the other hand, Fe-Au nanowires with a length of 1 μm and a diameter of 32.8 nm, coated with SH-PEG-COOH and Dop-PEG, were most appropriate as T2 contrast agents, being comparable to commercial Fe oxide nanoparticles. The authors also performed a MRI of some samples containing Fe and Fe-Au nanowires (Fig. 23), at a magnetic field of 9.4 T, in order to confirm the contrast caused by the nanostructures in the image.

A distinct approach, also based on nanowires, was reported by Peci.[164] The author filled the central capillary of carbon nanotubes with continuous ferromagnetic α-Fe nanowires, producing a structure with two different competing anisotropy contributions that result in a small effective anisotropy, and functionalized their surface with paramagnetic Gd^{3+}. Then, these structures were analyzed as candidates for a dual approach, namely, magnetic hyperthermia cancer therapy and MRI contrast agents. In the context of MRI, the relaxivity of the filled carbon nanotubes was directly measured at magnetic fields of 9.4 T and 14 T. The acquired results demonstrated that these nanostructures are viable as high-relaxivity contrast agents for high-field MRI, having the largest relaxivity values when compared to all the candidates considered in the study for high-field T1 contrast.

In a different study by Cham-Fai and Wang[165] one-dimensional magnetic manganese (Mn)-Fe nanostructures, namely, nanoneedles, nanorods, and nanowires, were fabricated by self-assembly of Mn-doped iron oxide nanoparticles, using cystamine as the linker. Then, the suitability of these nanoarchitectures as MRI contrast agents was evaluated in a clinical 1.5 T whole-body magnetic resonance system. The obtained results showed that all the considered nanostructures had notable T2 relaxivities, especially the nanoneedles. In this work, a cell viability test was also performed, on a cell line established from a tumor induced by the Abelson murine leukemia virus (RAW264.7), and a growth curve was obtained, which indicated acceptable safety profiles for these nanoarchitectures.

A report by Corr *et al.*[145] addressed suspensions of linear arrays of magnetite nanoparticles, produced by the cross-linking of surrounding particles with polyelectrolyte molecules, in the context of this biomedical application. Through the application of an external magnetic field, it was verified that these nanostructures were rearranged into parallel arrays. The relaxivity of such nanostructures was measured using field-cycling NMR at 37 °C, and a considerable reduction in the relaxation times at all the considered fields was observed. The authors also acquired MR images of live rats, injected with these nanoarchitectures, in order to assess their effect on the brain. The obtained results demonstrated that these nanoarchitectures had good biocompatibility and potential as contrast agents for *in vivo* MRI, having darkened the brain regions reached in a T1-weighted image.

In addition to the previously addressed nanoarchitectures, SAF nanostructures have also been studied as potential contrast agents for MRI. Roosbroeck *et al.*[30] fabricated phospholipid-coated, disk-

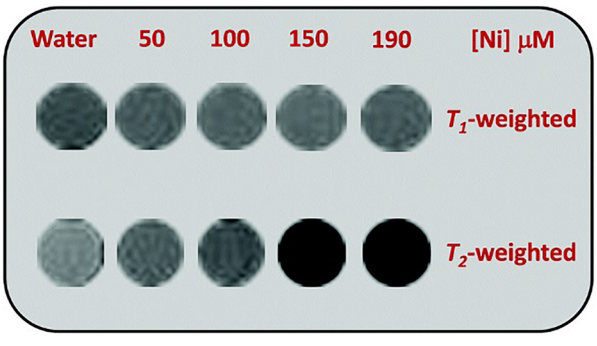

FIG. 22. MRI phantom image obtained using T1- and T2-weighted sequences at 3 T and 37 °C.[43] Reprinted with permission from Bañobre-López *et al.*, "A colloidally stable water dispersion of ni nanowires as an efficient t2-MRI contrast agent," J. Mater. Chem. B **5**, 3338–3347 (2017). Copyright 2017 Clearance Center, Inc.

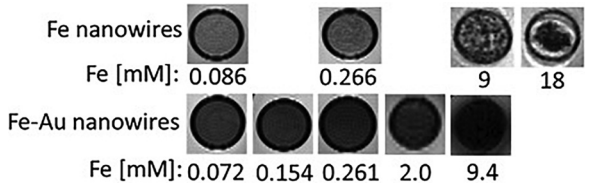

FIG. 23. T2-weighted images of samples containing Fe nanowires and Fe-Au nanowires.[42] Reprinted with permission from Shore *et al.*, "Electrodeposited fe and fe–au nanowires as MRI contrast agents," Chem. Commun. **52**, 12634–12637 (2016). Copyright 2016 Clearance Center, Inc.

shaped, and multilayered [Au(10 nm)/Ni_{80}Fe(5 nm)$_{20}$/Au(2.5 nm)/Ni_{80}Fe(5 nm)$_{20}$/Au(10 nm)] SAF nanoarchitectures, with diameters ranging from 89.8 nm to 523.2 nm, using a colloidal lithography technique. Magnetic characterization of these nanodiscs indicated a very low remanence value as well as a high magnetization, making them adequate for biomedical applications. Then, these nanostructures were evaluated as T2 contrast agents, showing improved relaxivities, at 24.85 °C in a 9.4 T magnetic field, when compared to the commercial options, especially the smallest particles with a diameter of 90 nm. The authors also carried out an *in vitro* MRI study (Fig. 24), using an ovarian cancer cell line (SKOV3,) confirming the increased T2 relaxation for cells marked with such nanostructures.

Antiferromagnetic nanoarchitectures were also studied as potential T1 contrast agents by different authors. Namely, Na *et al.*[166] fabricated antiferromagnetic MnO nanoparticles of different sizes, namely, 7, 15, 20, and 25 nm, coated with a PEG-phospholipid shell. The relaxivity of such particles was measured using a 3.0 T human clinical scanner, and their *in vivo* performance as MRI contrast agents was analyzed on a mouse. The obtained results indicate that these nanoparticles are suitable as T1 contrast agents, demonstrating no significant toxicity, for a MnO concentration less than 0.82 mM, in eight human cell lines originating from different tissues. Furthermore, by conjugating them with a tumor-specific antibody, it was possible to selectively improve the contrast of breast cancer cells located in a mouse's metastatic brain tumor, which was intravenously injected with the functionalized nanoparticles, through T1-weighted MRI.

Neves *et al.*[167] addressed these nanoparticles (average size of ~20 nm) as well; however, in this case, they were coated with carboxymethyl-dextran and the *in vivo* study was not performed. Nevertheless, the authors also considered them adequate as T1 contrast agents, due to the significant longitudinal relaxivity measured on a clinical 3.0 T MRI scanner. Moreover, it was observed that such nanoparticles present no *in vitro* cytotoxicity for healthy cells at concentrations lower than 25 μg/ml; however, for HeLa cells, a notable toxicity was observed even at low concentrations of nanoparticles (5 μg/ml).

On a different work, Peng *et al.*[168] fabricated and studied another T1 contrast agent, known as antiferromagnetic α-iron oxide-hydroxide nanocolloids, with a diameter of 2–3 nm, which were prepared in the mesopores of wormlike mesoporous silica. The relaxation times, measured at 40 °C using a 0.47 T Minispec spectrometer, indicated that these nanoparticles had the lowest T2 relaxivity/T1 relaxivity ratio reported, until 2013, for iron-based colloidal T1 contrast agents, and possessed a considerably high longitudinal relaxivity. Additionally, the acquired MR images showed that such nanocolloids are a superior T1 contrast agent in both *in vitro* (HeLa cells) and *in vivo* (rat and mouse) MRI, when compared to ultrasmall iron oxide nanoparticles. Furthermore, these nanocolloids also demonstrated a high level of biocompatibility and biodegradability.

C. Magnetomechanical induced cellular annihilation

The current cancer treatment techniques, such as surgery, radiotherapy, and chemotherapy, are highly aggressive to the organism due to their invasiveness as well as possible side effects.[169] Therefore, it would be beneficial to the patient if the shortcomings associated with those therapies could be surpassed.[170] In this context, the different properties of nanomaterials have been studied and considered as a potential path for next generation oncologic treatments.[169] Particularly, there exists increasing interest in the use of magnetic nanostructures to mechanically stimulate and destroy specific cells since magnetic nanomaterials can be remotely controlled by applying

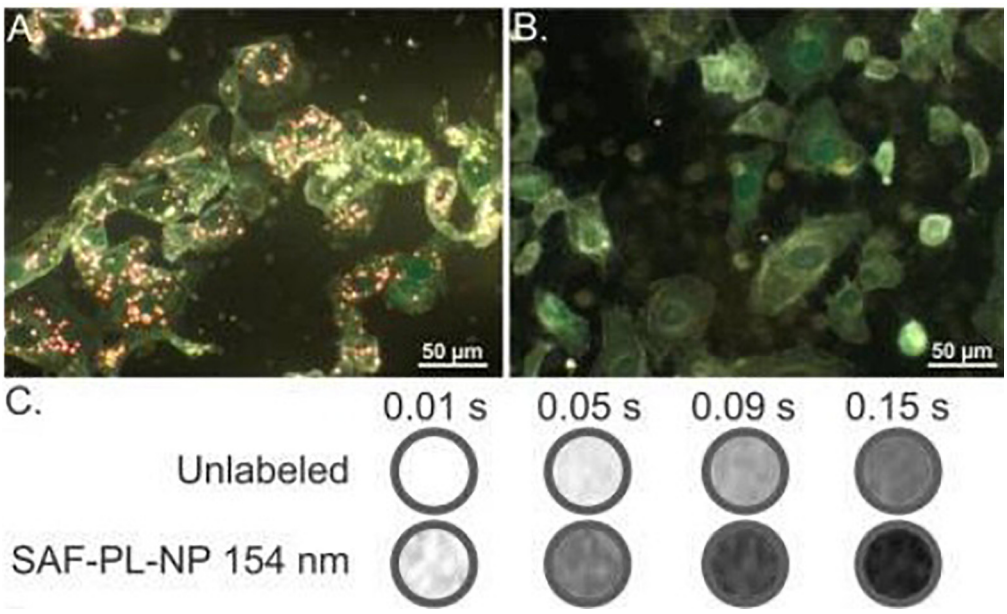

FIG. 24. (A) Dark-field image of SKOV3 cells after overnight incubation with 154 nm phospholipid-coated SAF nanoparticles (SAF-PL-NPs). (B) Dark-field image of unlabeled SKOV3 cells. (C) MRI images of labeled and unlabeled SKOV3 cells at various echo times.[30] Reprinted with permission from Roosbroeck *et al.*, "Synthetic antiferromagnetic nanoparticles as potential contrast agents in MRI," ACS Nano **8**, 2269–2278 (2014). Copyright 2014 American Chemical Society.

external magnetic fields and also due to the fact that cells convert mechanical stimuli into biochemical signals, via a process known as mechanotransduction.[38,170–172]

Therefore, the capacity to manipulate the cellular signals through the use of magnetic nanomaterials and external magnetic fields opens up multiple possibilities for the development of new treatment techniques.[38] Most of the experimental studies performed use superparamagnetic nanoparticles; however, their reduced saturation magnetization implies that high magnetic fields must be applied in order to manipulate them.[170] A particularly interesting alternative is known as magnetomechanical induced cell death.[170] This technique consists in exerting forces or torques on cells, using magnetic nanoarchitectures controlled by low frequency magnetic fields, in order to induce cell apoptosis, i.e., the programmed cell death.[171,173]

The basis of magnetomechanical actuation in cells is the spatial rotation that the magnetic nanostructures perform, in order to align themselves with an applied magnetic field, through the Brown relaxation process. Consequently, it produces a magnetic torque that depends on the applied magnetic field characteristics as well as on the magnetic moment and magnetic susceptibility of the nanoarchitectures.[170,171]

This novel approach is promising as a new cancer therapy since it has various advantages when compared to other techniques, namely, the possibility to specifically target cancer cells by functionalizing the surface of the magnetic nanostructures, which would significantly reduce the toxic side effects of chemotherapy, as well as the considerably lower strength and frequency of the required magnetic field in comparison to hyperthermia, making it easier to implement while eliminating the risk of destroying healthy tissues by undesired local overheating.[171,174] Therefore, various studies, driven by the improvement of such a technique, have addressed the application of different magnetic nanoarchitectures in this biomedical application. The typical characteristics of such nanostructures are a high saturation magnetization and low field magnetic susceptibility as well as a reduced remanence, for the fact that they will require lower magnetic fields for manipulation and will not agglomerate in the absence of a magnetic field.[169,170,175,176]

Micro/nanodiscs in a spin vortex state, i.e., an in-plane flux-closure spin distribution, are a particular interesting material for this biomedical application since they present no remanence and have a large single domain, when compared to the typical superparamagnetic particles.[34,177] The first reported experimental study addressing this particular technique with such nanostructures was carried out by Kim *et al.*[34]

In that work, Permalloy microdiscs in a spin vortex ground state, with a thickness of 60 nm and a diameter of ∼1 μm and coated on both sides with a 5 nm thick gold layer (for biocompatibility and surface modification), were prepared by magnetron sputtering and optical lithography. Afterward, the surface of these disks was functionalized with an antibody that recognizes a receptor overexpressed on the surface of glioma cells (IL13 α 2r), in order to specifically target human glioblastoma multiforme cells (N10 glioma cancer cells), an aggressive form of brain cancer. After the incorporation of the functionalized microdiscs by the cells (average of 10 disks per cell), they were exposed to spatially uniform alternating current (AC) magnetic fields with different intensities and frequencies (Fig. 25). The obtained results show that biologically relevant cell damage (∼90% cell death) was achieved by considerably weak magnetic fields (<10 mT), with frequencies of a few tens of Hertz (10–20 Hz), applied only for 10 min. Therefore, this technique has a strong contrast to the typical heating-induced cell toxicity using superparamagnetic particles, where considerably stronger AC magnetic fields, with frequencies of hundreds of kilohertz, are required.[34]

Similar studies were performed by Rozhkova *et al.*,[178] Novosad and Rozhkova,[179] and Vitol *et al.*;[175] however, in the latter case, a different cell line, namely, A172 glioblastoma cells, was exposed for 15 min to a 10 mT AC magnetic field, with a frequency of 10 Hz, and a magnetomechanically induced controlled drug release was also addressed. Even so, the results acquired in the magnetomechanical induced cell death by the various authors were similar to the ones obtained in the work performed by Kim *et al.*[34]

On a different study by Leulmi *et al.*,[171] three types of disk-shaped anisotropic magnetic particles were prepared and characterized, namely, synthetic antiferromagnetic (SAF), vortex, and polycrystalline magnetite particles with random anisotropy. All these structures had a diameter of 1.3 μm and, similar to the previous studies, were coated with gold layers. Afterward, the magnetic properties of the various fabricated particles, as well as their deposition process, were compared and the vortex configuration was considered the best option to start an *in vitro* study on the magnetomechanical effect in human renal carcinoma cells, due to their magnetic softness and ease of fabrication.

Therefore, the surface of these microdiscs was functionalized with ligands in order to target specific renal cancer cells (SKRC-59) during their incubation with the magnetic particles, reaching an average of 30 particles per cell. Then, an alternating magnetic field (30 mT) with a low frequency (∼20 Hz) was applied for 1 h, and the impact of the treatment was analyzed. The statistical results (shown in Fig. 26), obtained by measuring the proportion of the different categories of cells (live vs apoptotic vs necrotic) after the procedure, indicate a significant increase in the cancer cell death by apoptosis (∼70%), demonstrating that the method is capable of inducing the destruction of target cells *in vitro*. The authors also confirmed that the movement of magnetic particles linked to human renal carcinoma cells induces apoptosis, through the observation of caspase activation after a 45 min exposure to an identical AC magnetic field.

Cheng *et al.*[37] also studied the application of gold coated Permalloy microdiscs, with a spin-vortex state, in the magnetomechanical induced destruction of a human glioblastoma cell line (U87), demonstrating a distinct method for the *in vivo* destruction of those cells through the movement of the magnetic particles in a low frequency rotating magnetic field. The magnetic disks, fabricated by optical lithography followed by thermal evaporation, had a diameter of 2 μm and a thickness of 70 nm. The *in vitro* toxicity of these microdiscs was assessed on U87 glioma cells, loaded with the magnetic particles (average of 39 particles per cell), by exposing those cells to a low frequency (20 Hz) rotating magnetic field of 1 T for 30 min (Fig. 27). After this process, it was observed that up to 89% of the cells were nonviable. Additionally, a trypan blue exclusion test was performed in order to assess the integrity of the cellular membrane after a 5 min treatment. This assay demonstrated that, by applying a rotating magnetic field, such disks can generate enough mechanical force to affect the structure of the cell's membrane, causing extensive cell death.

The magnetomechanical effect of these particles was also assessed *in vivo* by implanting U87 glioma cells, preincubated for 24 h prior to

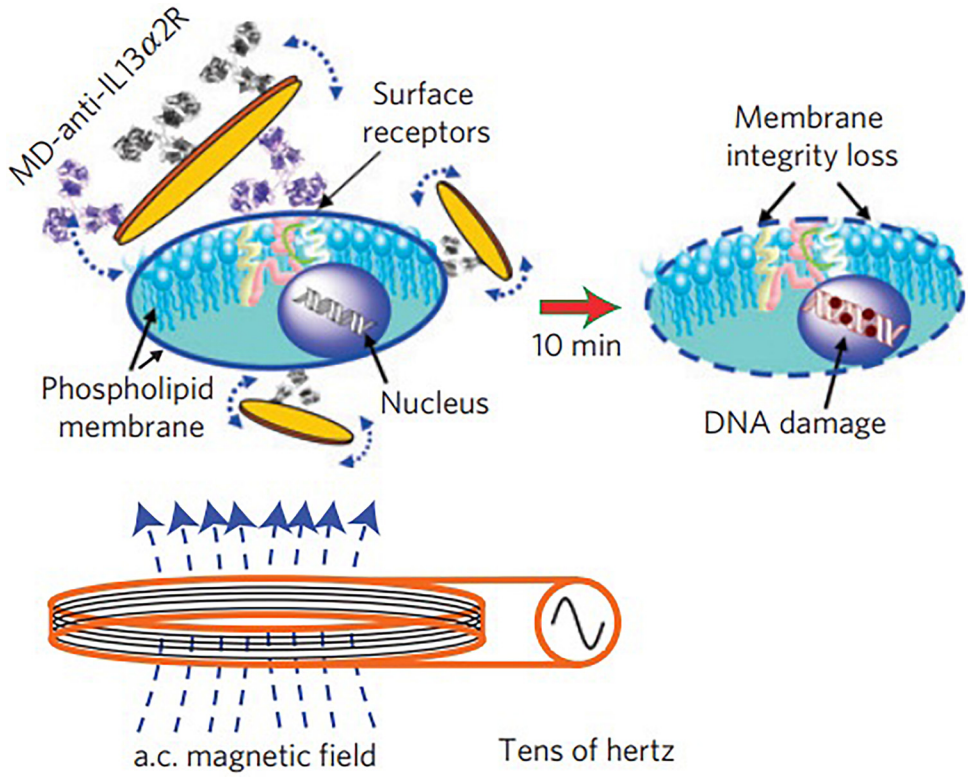

FIG. 25. The idea of targeted magnetomechanical cancer cell annihilation employing disk-shaped magnetic structures with a spin-vortex ground state.[34] Reprinted with permission from Kim *et al.*, "Biofunctionalized magnetic-vortex microdiscs for targeted cancer-cell destruction," Nat. Mater. **9**, 165–171 (2010). Copyright (2009) Springer Nature Customer Service Center GmbH: Springer Nature.

injection with magnetic microdiscs at a ratio of 50 particles per cell, on mice. In this case, a low frequency rotating magnetic field, with identical characteristics, was applied daily for 1 h during 7 days. After the treatment, a reduced tumor size as well as an improved survival rate for the treated glioma bearing mice was verified, indicating that these disks can damage cancer cells *in vivo* when a magnetic field is applied.

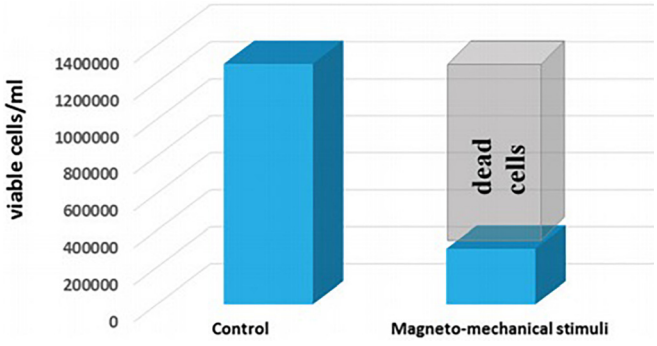

FIG. 26. Cancer cell viability after exposure to an AC magnetic field for 45 min.[171] Reprinted with permission from Leulmi *et al.* "Triggering the apoptosis of targeted human renal cancer cells by the vibration of anisotropic magnetic particles attached to the cell membrane," Nanoscale **7**, 15904–15914 (2015). Copyright 2015 Clearance Center, Inc.

In order to get a better understanding of the *in vivo* cell destruction mechanism and address a more realistic approach, the microdiscs were injected inside an established tumor, at a ratio of 50:1 magnetic particles to injected cell, and then a rotating magnetic field (1 T) with a frequency of 20 Hz was applied daily for 1 h during 7 days. The brain tissues, acquired after the treatment and examined by histology studies, showed an increase in the intratumoral apoptosis on the treated mice, suggesting that the movement of the magnetic structures in the rotating magnetic field is sufficient to damage the cancer cells *in vivo* and activate their apoptosis.

Searching for new paths, Goiriena-Goikoetxea *et al.*[44,180] studied the possibilities that arise in this biomedical topic when the dimensions of the microdiscs are reduced to the nanoscale. Driven by such a goal, the authors performed a comparison between the magnetomechanical interactions of Permalloy (Py) magnetic microdiscs (radius of 1 μm and thickness of 60 nm) and nanodiscs (radius of 70 nm and thickness of 50 nm), in a spin-vortex state, with human lung cancer cells (A549). Consequently, several aspects related to the interaction of those magnetic structures with cells were analyzed, namely, the internalization process, their cytotoxicity, and the magnetomechanical stimulus. In order to compare the internalization of the disks by the cancer cells, they were coated with a biocompatible material, namely, gold for the nanodiscs and gold or titanium for the microdiscs. To ease the internalization by the lung carcinoma cells, they were not functionalized. The obtained results showed that the number of cells

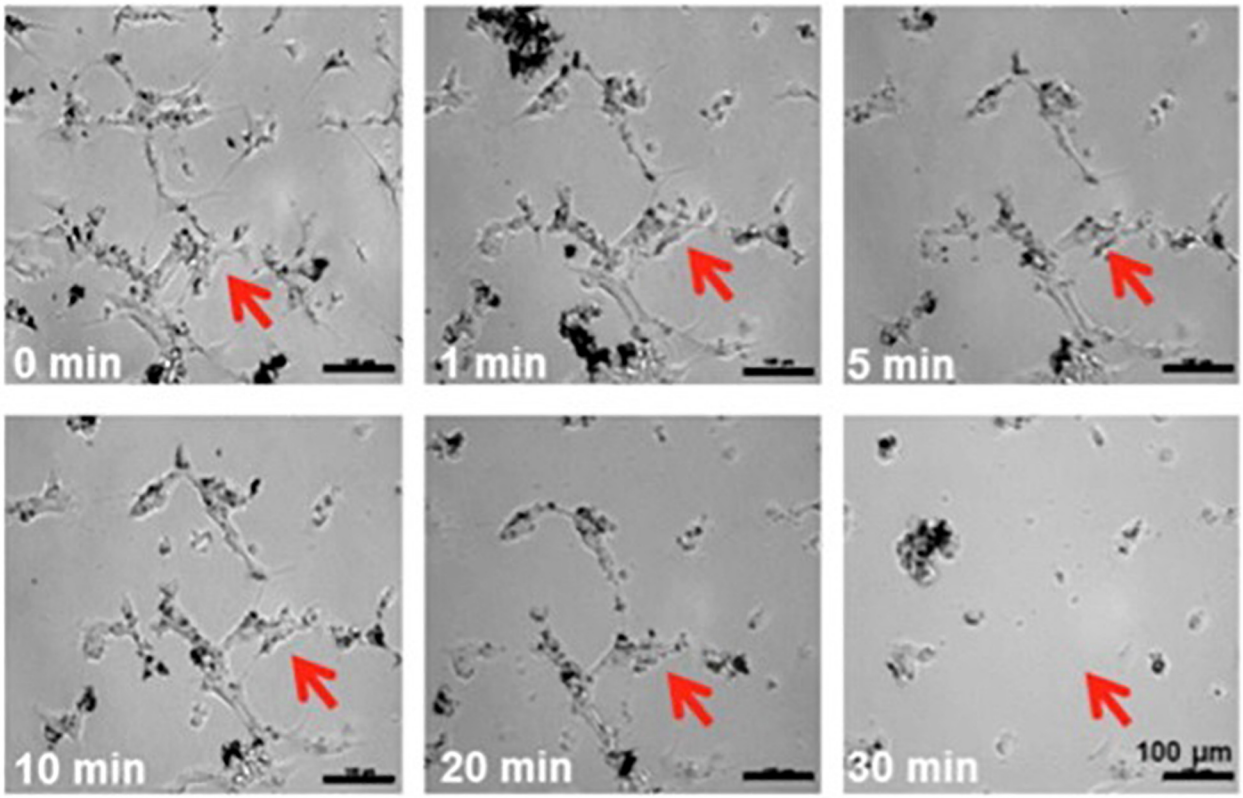

FIG. 27. Images of U87 cells, loaded with microdiscs, acquired from 0 min to 30 min after the treatment. The red arrow shows that the same area was tracked.[37] Reprinted with permission from Cheng *et al.*, "Rotating magnetic field induced oscillation of magnetic particles for *in vivo* mechanical destruction of malignant glioma," J. Controlled Release **223**, 75–84 (2015). Copyright 2015 Elsevier.

with internalized nanodiscs (average of 100 per cell) is a little higher when compared to the ones having microdiscs (average of 6 per cell). This probably occurs due to the improved distribution of nanodiscs within the medium.

In the following, and before the study of the magnetomechanical cell damage caused by the nanostructures, their cytotoxic effect was evaluated on the lung carcinoma cells.[44,180] For that purpose, a nominal proportion of 25 microdiscs and 2000 nanodiscs per cell was added and, after incubation, the vital functions of the cells, as well as their proliferation rates, were analyzed (see Fig. 28). The obtained results demonstrated that the disks do not affect the viability of the cells; however, they seemed to inhibit their proliferation. Finally, the efficiency of the magnetomechanically actuated micro- and nanodiscs in the destruction of cancer cells was analyzed. This study was performed by exposing the cancer cells, previously incubated for 24 h with a nominal proportion of 25 titanium-coated microdiscs or 2000 gold-coated nanodiscs per cell, to a 10 mT AC magnetic field, with a frequency of 10 Hz, for 30 m. 4 h after this process, a 15% viability reduction among the cells that internalized microdiscs was observed. On the other hand, for the cells with internalized nanodiscs, it was verified that 30% died. Consequently, this proves that nanodiscs can also cause irreparable damage in the integrity of cancer cells, in spite of the reduced number of experiments performed as well as the lack of a cytometer. The increased cell death caused by the nanodiscs was not explicitly addressed by the authors; nevertheless, it was verified that when a magnetic field was applied, the nanodiscs formed chains, and then, when the field was turned off, those chains broke quickly and the nanostructures redispersed, as opposed to the microdiscs, which continued to form chains in the absence of a magnetic field. This chaining and redispersion of the nanodiscs, originated by an AC magnetic field, could possibly cause the disruption of the lysosomal membrane, where the nanostructures are accumulated, liberating lysosomal hydrolases into the cytosol and activating cell death.

Besides disk-shaped magnetic nanostructures, other types of magnetic nanoarchitectures and magnetic fields have been studied in the context of magnetomechanical induced cell death. An example is the work of Wong *et al.*,[170] where biaxial pulsed magnetic fields (14 ± 1mT; 1–20 Hz) were applied to suspensions of HeLa cells having a concentration of 0.1 mg/ml of magnetic nanostructures for 10 min. In this work, the analyzed nanoarchitectures, which presented a triple vortex state, had three different diameters, namely, 150 nm, 250 nm, or 350 nm, and a length of 500 nm. On one hand, the cell apoptosis caused by uniaxial AC and direct current (DC) pulsed magnetic fields was compared against the one obtained from the biaxial pulsed fields, considering the particles with a diameter of 150 nm [Fig. 29(a)]. In this context, it was verified that a larger magnetic torque, demonstrated by a higher responsiveness over a wide range of frequencies, is induced on the nanostructures by applying a biaxial pulsed magnetic field,

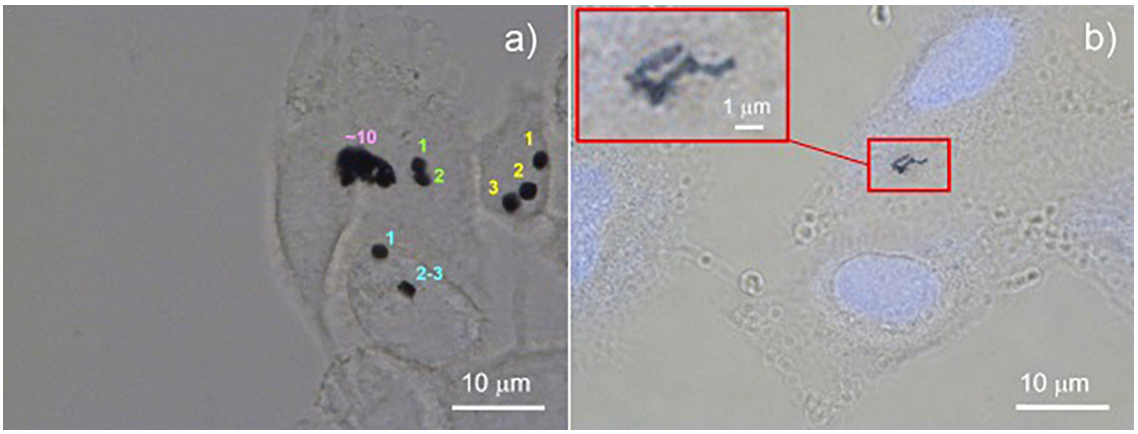

FIG. 28. Micrographs of lung carcinoma cells after 24 h of incubation with (a) microdiscs (coated with gold) and (b) nanodiscs (coated with gold).[44] Reprinted with permission from M. G. Goikoetxea, "Magnetic vortex nanodiscs for cancer cell destruction," Ph.D. thesis (Universidad del País Vasco-Euskal Herriko Unibertsitatea, 2017).Copyright 2017 Author licensed under a Creative Commons Attribution (CC BY-NC-SA 3.0 ES) license.

resulting in an increased *in vitro* magnetomechanical induced cell death. This study also concluded that the nanoarchitecture with the smaller diameter had the greatest low field susceptibility and remanence, therefore allowing the application of larger forces to the cells. This was confirmed in the cell viability test performed, where the particles with a diameter of 150 nm produced more 12% cell death when compared to the remaining nanostructures, which caused a cellular mortality of around 20% at best, under identical conditions [Fig. 29(b)].

Magnetic nanowires have also been studied in the context of magnetomechanical induced cell damage by various authors. One of the first reports addressing this one-dimensional nanostructure in such biomedical application is by Fung *et al.*[181] In their work, ferromagnetic Ni nanowires, with diameters ranging from 198 nm to 280 nm and an average length of 4.4 μm presenting longitudinal magnetic anisotropy, were prepared by electrodeposition in porous aluminum oxide templates and then incubated with fibroblast (NIH/3T3) for about 12 h (Fig. 30). These nanostructures did not significantly affect the cell viability in the absence of a magnetic field, in spite of Ni being an agent of hypersensitivity and moderately cytotoxic. Then, the nanowires were exposed to a weak (240 mT) and low-frequency (1 Hz) rotating magnetic field for 20 min. After this process, a viability reduction of the cell cultures by 89% was observed, indicating that this process effectively induced cell death.

Complementing this work, Choi *et al.*[182] demonstrated the death of human embryonic kidney cells (HEK-293) due to the rotation of internalized Ni nanowires, with an average nominal diameter of 150 nm and longitudinal magnetic anisotropy, caused by the application of an external AC magnetic field. In this study, it was also verified that the AC modulation amplitude and rate were fundamental parameters to determine the rotation of the nanowire inside the cell; however, the authors do not specify field intensity and frequency or the cell death rate achieved using this technique.

Also, in this context, Contreras *et al.*[183] analyzed the magnetomechanical effect in human colon cancer cells (HCT116) incubated with two concentrations of Ni nanowires (2.4 and 12 μg/ml). These nanostructures had a diameter of 35 nm and a length of 4 μm and presented longitudinal magnetic anisotropy. After the incubation, the viability of the cells was confirmed, and subsequently, they were exposed to an AC magnetic field (0.5 mT; 1 Hz or 1 kHz) for 10 or 30 min. Similar to the previous reports,[182,184] after the application of the magnetic field, a drop in the cell viability was verified, with a maximum decrease of 38% for the concentration of 12 μg/ml and the magnetic field of 1 kHz being observed. It was also demonstrated that there was no significant difference between applying the process for 10 min or 30 min, which indicates that the cell death induction mechanisms affect cells fast.

A different study by Contreras[184] considered the application of Fe and Ni nanowires, with longitudinal shape anisotropy, in the same experimental conditions, and revealed that the first nanostructures are better tolerated by the used cell lines (HCT 116 and HeLa). Different lengths of nanowires (1 μm and 5 μm) were also analyzed; however, a significant influence of this parameter on the cell viability for nanostructures of the same material was not observed. Afterward, both types of nanowires (with a diameter of 35 nm and ~4 μm long) were incubated with cells (HCT 116) at two different nanowire-to-cell concentrations (100:1 and 500:1), and then AC magnetic fields (0.5 mT and 1 Hz or 1 kHz) were applied. Similar to the previous study, it was verified that the magnetomechanical action resulted in the death of up to 60% of cancer cells when using Ni nanostructures at a 500:1 concentration, with a 1 h exposure. Additionally, it was found that a one hour incubation time seemed to be optimal for the application of this treatment.

Bearing in mind the improvement of this particular application for magnetic nanowires, Martínez-Banderas *et al.*[169] developed a bimodal strategy to induce cancer cell death through the combination of the chemotoxic effect caused by an anticancer drug (doxorubicin) with the mechanical perturbation exerted by Fe nanowires (average length of 6.4 $\pm$1.3 μm and a diameter of 30 to 40 nm) exposed to a low frequency (10 Hz) AC magnetic field (1 mT) for 10 min. The one dimensional nanostructures, shown in Fig. 31, were coated with 3-aminopropyltriethoxysilane (APTES) or with bovine serum albumin (BSA), in order to allow their functionalization with doxorubicin (DOX).

The efficiency of this technique in cell death induction was determined by the viability reduction of breast cancer cells (MDA-

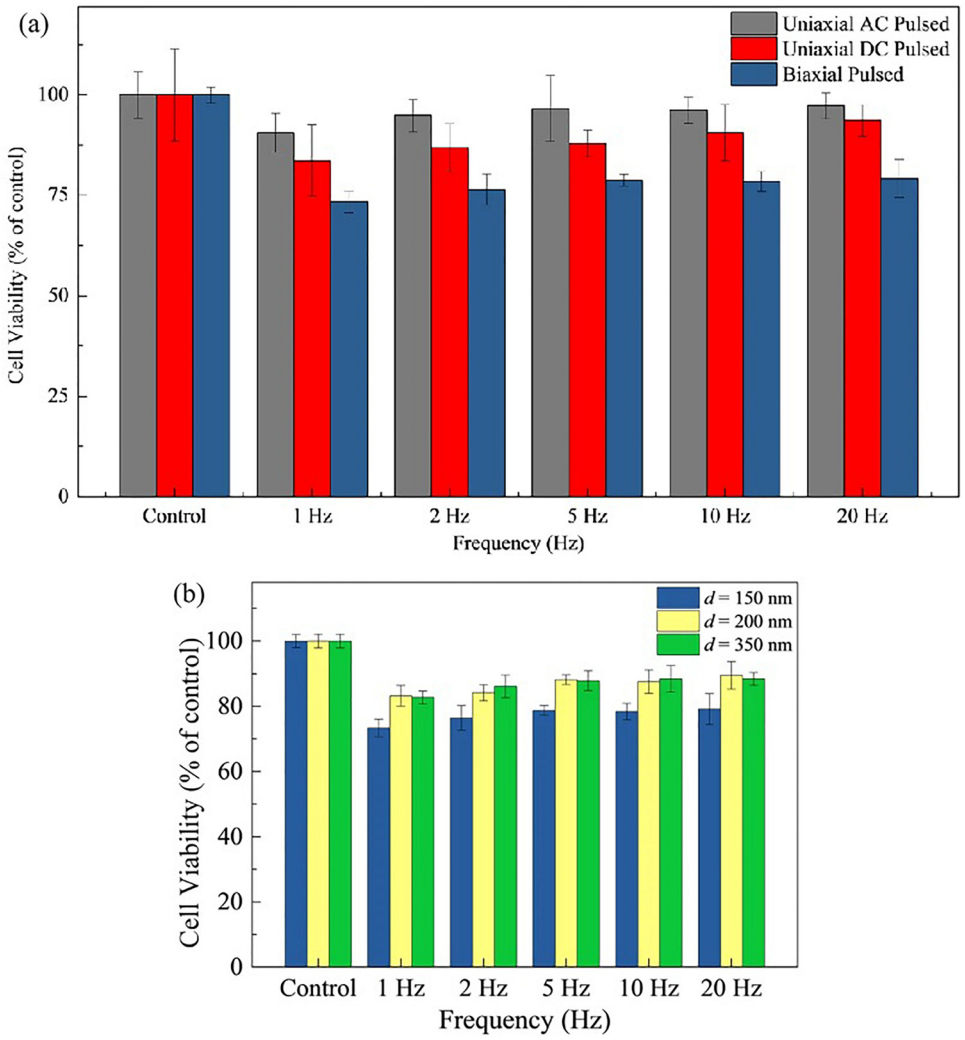

FIG. 29. (a) HeLa cell viability after magnetomechanical treatment for different magnetic field configurations. (b) Comparison of HeLa cells' viability after magnetomechanical cell annihilation treatment using nanostructures with d = 150–350 nm and l = 500 nm.[170] Reprinted with permission from Wong *et al.*, "Magneto-actuated cell apoptosis by biaxial pulsed magnetic field," Sci. Rep. **7**, 10919 (2017); Copyright 2017 Authors licensed under a Creative Commons Attribution (CC BY 4.0) license.

MB-231). The nanostructures were incubated with the cells at a concentration of 0.05 mg Fe/mL for 24 h, and it was verified that the functionalized nanowires demonstrated a high degree of internalization by the cells, becoming efficient carriers for drug delivery. The nanowires coated with BSA showed better internalization (26 ± 3 pg of Fe per cell) and a wider distribution within the cells, besides forming smaller and less compact clusters. Consequently, these were considered a more efficient option for the induction of cellular death. In this work, a large cytotoxic effect in the breast cancer cells caused by the dual effect of the functionalized nanowires was also observed, with a maximum reduction of 73% in cell viability, when using BSA-coated nanostructures. Therefore, it was demonstrated that the combination of the chemotoxic and magnetomechanical treatment modes, using magnetic nanowires, had synergistic effects, turning this technique into an attractive approach for novel cancer therapies.

Serrà *et al.*[185] approached this theme on a different perspective by fabricating multisegmented, nontoxic, and biocompatible $(Au/Ni\text{-}NiO)_8$ nanowires, with longitudinal magnetic anisotropy, through a single-bath potentiostatic-pulsed electrodeposition process. These nanostructures have a triple functionality since they can carry two types of functional molecules and induce cell death by magnetic actuation. The HeLa cells were incubated with nanowires at different concentrations ($0 - 200\ \mu$g/ml), and after internalization and cytotoxicity assessment, AC magnetic fields with a frequency of 20 Hz and strengths ranging from 2 to 40 mT were applied. These caused the nanostructures to vibrate and move inside the cells favoring the release of the drugs that they carried. After this process, it was verified that the motion of the nanowires induced the apoptosis of the HeLa cells, without evidence of mechanical destruction. It was also shown that the cell death increased for higher magnetic field strengths. Therefore,

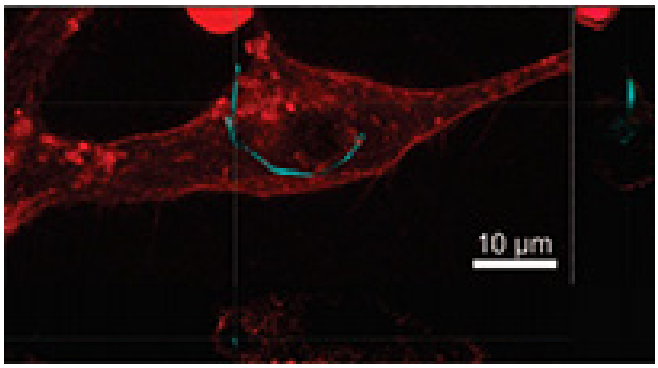

FIG. 30. Confocal projection and cross sections of a 3T3 fibroblast (red) with various Ni nanowires internalized (blue).[181] Reprinted with permission from Fung *et al.*, "Induction of cell death by magnetic actuation of nickel nanowires internalized by fibroblasts," J. Phys. Chem. C **112**, 15085–15088 (2008). Copyright 2008 American Chemical Society.

these multisegmented nanostructures provide a novel platform that induces the death of cancer cells, combining a magnetomechanically action with drug release.

Besides nanowires and disks in a spin-vortex state, some studies also analyzed the suitability of SAF nanostructures for magnetomechanical induced cell death. An example is the report by Mansell *et al.*[35] where disk-shaped SAFs (2 μm diameter), with perpendicular magnetic anisotropy, were fabricated from a repeated motif of ultrathin CoFeB/Pt layers and then applied in an *in vitro* study with glioma cells. The efficiency of the CoFeB/Pt microdiscs in this biomedical application was compared against the one obtained from Py spin-vortex microdiscs, which have an easy magnetization plane, on the same conditions (Fig. 32).

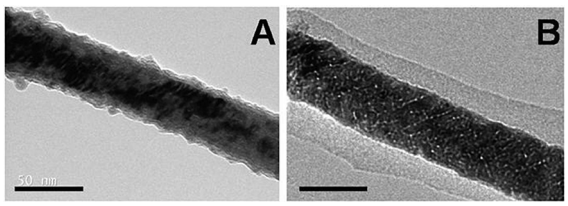

FIG. 31. TEM micrographs of (A) APTES-coated nanowires and (B) BSA-coated nanowires. The scale bars are equal to 50 nm.[169] Reprinted with permission from Martínez-Banderas *et al.*, "Functionalized magnetic nanowires for chemical and magneto-mechanical induction of cancer cell death," Sci. Rep. **6**, 1–11 (2016). Copyright 2016 Authors licensed under a Creative Commons Attribution (CC BY 4.0) license.

In this case, brain tumor cells (U87) were incubated for 24 h at a concentration of 50 particles per cell. The cell damage was quantified after the application of a rotating (20 Hz) magnetic field (1 T) for one minute. It was verified that the CoFeB/Pt microdiscs were able to induce cellular death on 62 ± 3% of the cancer cells; however, under the same conditions, the Py microdiscs could only kill 12 ± 2% of the glioblastoma cells. The torque applied by the two types of particles was also measured, having maximum values of 20 fNm for CoFeB/Pt and 75 fNm for the Py nanostructures. Therefore, it was shown in this work that the symmetry of the anisotropy is more relevant than the magnitude of the torque in causing effective cell destruction. Consequently, the ability to explore the anisotropy of nanostructures can open new paths for the magnetomechanical induced cell death.

Kwon[186] also performed a work where disk-shaped SAF nanostructures, based on Fe_3O_4, were fabricated and then studied the context of magnetomechanically induced cell death (HeLa cell line) through the application of an AC magnetic field (200 mT; 1 Hz). The author assessed the effect of the nanodisc concentration as well as

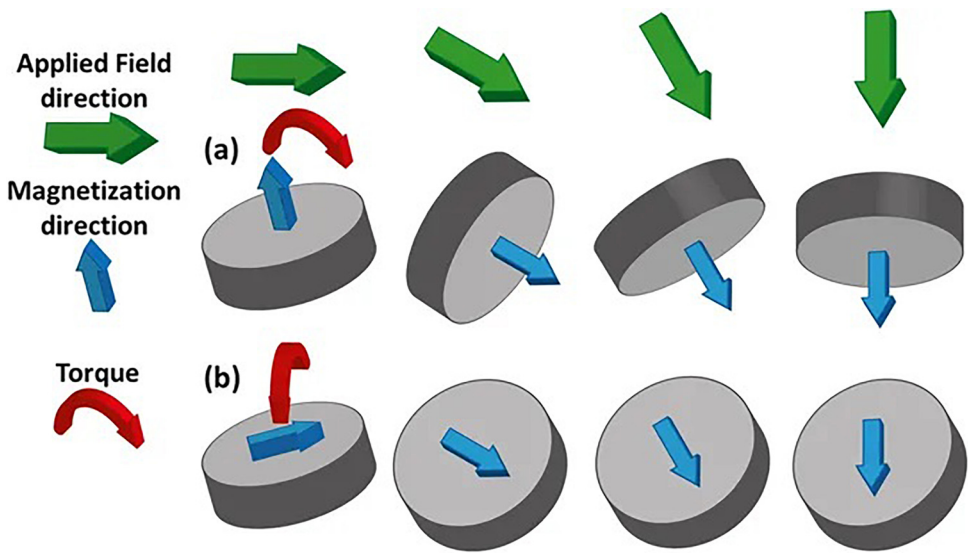

FIG. 32. Illustration demonstrating the magnetization direction and torques on (a) CoFeB/Pt particles and (b) Py vortex particles in a rotating magnetic field.[35] Reprinted with permission from Mansell *et al.*, "Magnetic particles with perpendicular anisotropy for mechanical cancer cell destruction," Sci. Rep. **7**, 4257 (2017). Copyright 2017 Authors Creative Commons Attribution (CC BY 4.0) license.

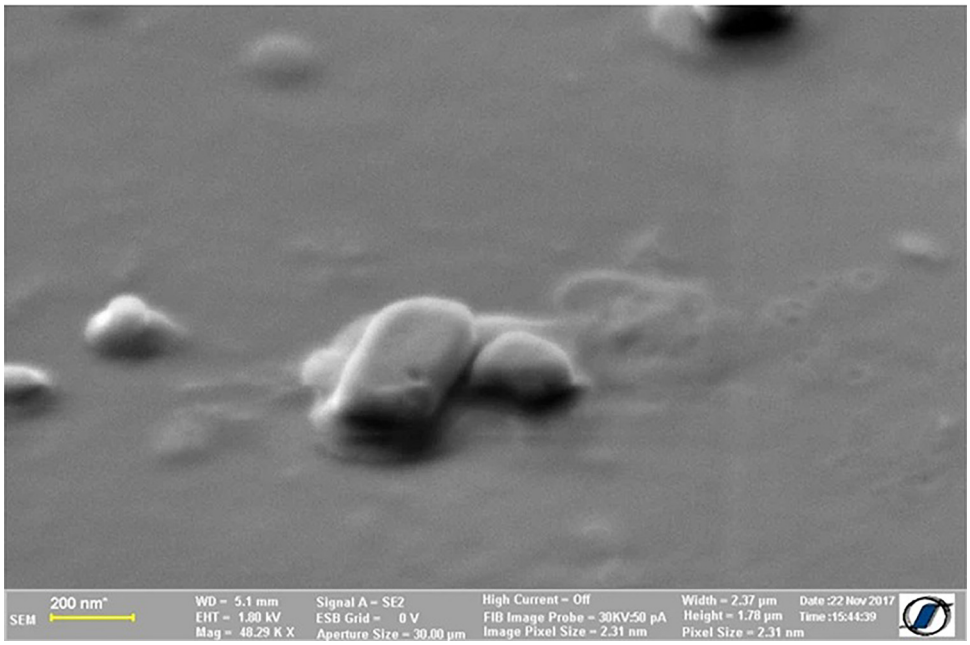

FIG. 33. SEM image of the rectangular-shaped magnetic nanoarchitectures.[117] Reprinted with permission from Chiriac *et al.*, "Fe-Cr-Nb-B ferromagnetic particles with shape anisotropy for cancer cell destruction by magneto-mechanical actuation," Sci. Rep. **8**, 11538 (2018).Copyright 2018 Authors licensed under a Creative Commons Attribution (CC BY 4.0) license.

the influence of treatment time on the cell viability. It was observed that cell viability decreases as the concentration of nanostructures increases; however, there is a "threshold" concentration (ratio of 1 nanoparticle: 4 cells) where the cell viability decreases abruptly. Additionally, it was verified that with 8 min of exposure, 80% of the cells were viable; however, after 16 min, less than 8% of them was alive. Therefore, the obtained results show that these nanoarchitectures, depending on the analyzed parameters, induce different levels of cell death when exposed to an AC magnetic field.

In the context of this biomedical application, a new type of rectangular-shaped magnetic nanoarchitecture, prepared by wet milling of superferromagnetic Fe-Cr-Nb-B precursor glassy ribbons (Fig. 33), was fabricated and studied by Chiriac *et al.*[117] These nanostructures possess an improved torque in a rotating magnetic field, due to the shape anisotropies induced not only by their shape but also by the superferromagnetism of the glassy alloys. To assess their effectiveness in cell death induction, human osteosarcoma cells (MG-63) were incubated with these nanostructures, at 5 different concentrations, 0.5, 1, 2, 3, and 5 mg of particles in 1 ml of cell culture, and afterward exposed to a rotating magnetic field for 10 min. The exposure time was also evaluated by exposing a nanostructure concentration of 2 mg/ml for 0, 5, 10, 15, and 20 min to the same magnetic field. Then, the cell viability (Fig. 34) was evaluated, and it was verified that the rotation of these nanoparticles caused relevant damage on the cells that increased with the increasing concentration and exposure time, in spite of the low intensity of the applied magnetic field (1 mT) at a frequency of 20 Hz. Therefore, these kinds of nanostructures can also be good candidate for the development of the magnetomechanically induced cell death technique.

A different approach was also reported by Shen *et al.*,[187] where cube-shaped iron oxide nanoparticles doped with zinc (Zn) were fabricated and then functionalized with the epidermal growth factor (EGF) peptide in order to target human glioblastoma cells (U87) *in vitro*. Consequently, after the incubation of the nanostructures with the cells at a concentration of 100 μg/ml, they were exposed to a low frequency (15 Hz) rotating magnetic field (40 mT) for 30 min per day for 3 days. It was verified that the application of the magnetic field resulted in the

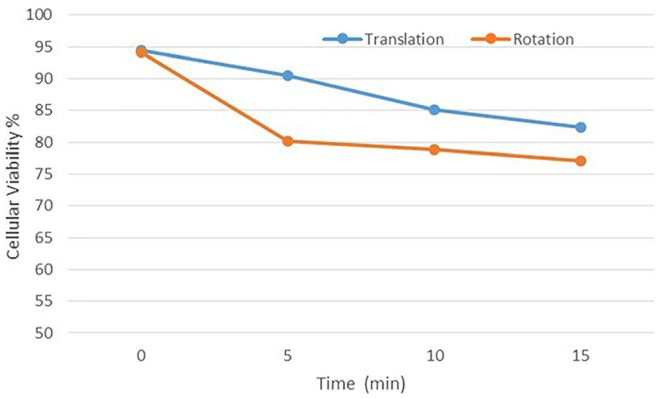

FIG. 34. Cellular viability of MG-63 cells, loaded with rectangular-shaped magnetic nanostructures, as a function of the exposure time to an AC magnetic field, which can cause their translation or rotation.[117] Reprinted with permission from Chiriac *et al.*, "Fe-cr-nb-b ferromagnetic particles with shape anisotropy for cancer cell destruction by magneto-mechanical actuation," Sci. Rep. **8**, 11538 (2018).Copyright 2018 Authors licensed under a Creative Commons Attribution (CC BY 4.0) license.

formation of elongated aggregates, with longitudinal magnetic anisotropy, which generated hundreds of pN. Afterward, the cell viability was assessed, and it was observed that more than 90% of the cells were damaged after the treatment, indicating that such clusters were in fact capable of inducing the destruction of cancer cells.

In this section, various works were addressed and some of them approached Ni nanomaterials in the context of magnetomechanical induced cellular annihilation. However, it was previously mentioned that Ni shows long term *in vitro* toxicity, which is a significant drawback for the *in vivo* application of such nanostructures. Consequently, one of the issues that future research in this field should address is the increase in the nanoarchitectures biocompatibility, which can open new paths for their clinical implementation.

Additionally, most of the studies described do not address *in vivo* situations, which are a key part for the development of nanostructures suitable for clinical application. A particularly important aspect is the biodistribution of those nanoarchitectures within an organism because we not only want them to reach the site of interest but also wish their removal from the body after the treatment. Searching through the literature, no studies were found on the *in vivo* biodistribution of magnetic nanoarchitectures. Until now, the *in vivo* biodistribution of nanomaterials is reported, mainly on mice and/or rat, for spherical magnetic nanoparticles,[188–194] carbon nanotubes,[195–202] and nanodiscs based on 11 α-helix MSP1E3D1 protein and 1-palmitoyl-2-oleoyl-sn-glycero-3-phosphatidylcholine lipids.[203]

From these works, it is possible to conclude that the upper and lower nanoparticle size limits are not precisely defined; however, various authors agree that the maximum dimension for a nanomaterial inside an organism should be around 150 nm, in order to avoid retention in the liver and spleen. On the other hand, the lower size limit is set by the glomerular filtration size cut-off of about 6 nm since we want to avoid renal elimination and consequently increase their circulation time inside the body, which leads to increased accumulation in target tissues.[189,204,205] Nevertheless, various studies include particles ranging up to the micrometer scale; however, it was observed that larger structures ($>1\ \mu$m) have the capacity to cause a partial or even total occlusion of the capillaries.[206,207] Throughout this section, different works were based on nanostructures with dimensions larger than 1 μm. Therefore, another path for the development of these biomedical applications can possibly be the reduction of the nanoarchitecture dimensions. Additionally, detailed *in vivo* studies addressing the effect of the magnetic nanostructure size on *in vivo* pharmacokinetics and cellular interaction should be performed, so that we can move a step closer toward the employment of these nanoarchitectures in real clinical cases.

With this review article, it was possible to address various promising biomedical applications of different magnetic nanostructures. These nanoarchitectures demonstrated considerable advantages when compared to the typical superparamagnetic nanoparticles. Nevertheless, there is also significant work left to do in this area, such as improving the magnetic nanostructures as well as get a better understanding of the interaction between biological systems and the nanoarchitectures. Therefore, it is expected that this theme will continue to be addressed by several authors over time, possibly leading to the development of new diagnostic and therapeutic techniques that can improve the life quality of the patients.

AUTHOR'S CONTRIBUTIONS

L.P. and R.M. contributed equally to this work.

ACKNOWLEDGMENTS

The authors acknowledge funding from the European Union's Horizon 2020 research and innovation program under the Marie Sklodowska-Curie Grant Agreement No. 734801. C.R. and R.M. acknowledge funding from Basque Government Grant Nos. PIBA 2018-11 and IT1162-19, and Spanish Grant No. FIS2016-76058 (AEI/FEDER, UE). D.N. acknowledges the Spanish Ministry for Science, Innovation and Universities, for funding through the "Ramón y Cajal" program RYC-2017-22820. C.T. Sousa thanks FCT for financial support through the Investigador FCT program (Contract No. IF/01159/2015). R. Magalhães is grateful to the FCT SFRH/BD/148563/2019 PhD grant. This work was also supported by the Portuguese Fundação para a Ciência e Tecnologia (FCT) and COMPETE 2020 (FEDER) under the projects POCI-01-0145-FEDER-028676/PTDC/CTM-CTM/28676/2017, POCI-01-0145/FEDER-032257/PTDC/FIS-OTI/32257/2017, POCI-01-0145-FEDER-031302/PTDC/FIS-MAC/31302/2017, and POCI-01-0141-FEDER-032527.

REFERENCES

[1]R. L. Stamps, S. Breitkreutz, J. Åkerman, A. V. Chumak, Y. Otani, G. E. W. Bauer, J.-U. Thiele, M. Bowen, S. A. Majetich, M. Kläui, I. L. Prejbeanu, B. Dieny, N. M. Dempsey, and B. Hillebrands, "The 2014 magnetism roadmap," J. Phys. D: Appl. Phys. **47**, 333001 (2014).
[2]D. Sander, S. O. Valenzuela, D. Makarov, C. H. Marrows, E. E. Fullerton, P. Fischer, J. McCord, P. Vavassori, S. Mangin, P. Pirro, B. Hillebrands, A. D. Kent, T. Jungwirth, O. Gutfleisch, C. G. Kim, and A. Berger, "The 2017 magnetism roadmap," J. Phys. D: Appl. Phys. **50**, 363001 (2017).
[3]S. Piramanayagam and K. Srinivasan, "Recording media research for future hard disk drives," J. Magn. Magn. Mater. **321**, 485–494 (2009).
[4]R. P. Cowburn, "Room temperature magnetic quantum cellular automata," Science **287**, 1466–1468 (2000).
[5]S. S. P. Parkin, M. Hayashi, and L. Thomas, "Magnetic domain-wall racetrack memory," Science **320**, 190–194 (2008).
[6]D. A. Allwood, "Magnetic domain-wall logic," Science **309**, 1688–1692 (2005).
[7]I. M. Miron, K. Garello, G. Gaudin, P.-J. Zermatten, M. V. Costache, S. Auffret, S. Bandiera, B. Rodmacq, A. Schuhl, and P. Gambardella, "Perpendicular switching of a single ferromagnetic layer induced by in-plane current injection," Nature **476**, 189–193 (2011).
[8]L. Liu, C.-F. Pai, Y. Li, H. W. Tseng, D. C. Ralph, and R. A. Buhrman, "Spin-torque switching with the giant spin hall effect of tantalum," Science **336**, 555–558 (2012).
[9]A. Fert, V. Cros, and J. Sampaio, "Skyrmions on the track," Nat. Nanotechnol. **8**, 152–156 (2013).
[10]A. D. Kent and D. C. Worledge, "A new spin on magnetic memories," Nat. Nanotechnol. **10**, 187–191 (2015).
[11]R. Wiesendanger, "Nanoscale magnetic skyrmions in metallic films and multilayers: A new twist for spintronics," Nat. Rev. Mater. **1**, 16044 (2016).
[12]O. Tegus, E. Brück, K. H. J. Buschow, and F. R. de Boer, "Transition-metal-based magnetic refrigerants for room-temperature applications," Nature **415**, 150–152 (2002).
[13]O. Gutfleisch, M. A. Willard, E. Brück, C. H. Chen, S. G. Sankar, and J. P. Liu, "Magnetic materials and devices for the 21st century: Stronger, lighter, and more energy efficient," Adv. Mater. **23**, 821–842 (2010).
[14]V. Franco, J. Blázquez, J. Ipus, J. Law, L. Moreno-Ramírez, and A. Conde, "Magnetocaloric effect: From materials research to refrigeration devices," Prog. Mater. Sci. **93**, 112–232 (2018).

[15]D. L. Graham, H. A. Ferreira, and P. P. Freitas, "Magnetoresistive-based biosensors and biochips," Trends Biotechnol. **22**, 455–462 (2004).
[16]R. S. Gaster, L. Xu, S.-J. Han, R. J. Wilson, D. A. Hall, S. J. Osterfeld, H. Yu, and S. X. Wang, "Quantification of protein interactions and solution transport using high-density GMR sensor arrays," Nat. Nanotechnol. **6**, 314–320 (2011).
[17]Y.-T. Chen, A. G. Kolhatkar, O. Zenasni, S. Xu, and T. R. Lee, "Biosensing using magnetic particle detection techniques," Sensors **17**, 2300 (2017).
[18]A. Fernandez-Pacheco, R. Streubel, O. Fruchart, R. Hertel, P. Fischer, and R. P. Cowburn, "Three-dimensional nanomagnetism," Nat. Commun. **8**, 15756 (2017).
[19]A. G. Roca, R. Costo, A. F. Rebolledo, S. Veintemillas-Verdaguer, P. Tartaj, T. González-Carreño, M. P. Morales, and C. J. Serna, "Progress in the preparation of magnetic nanoparticles for applications in biomedicine," J. Phys. D: Appl. Phys. **42**, 224002 (2009).
[20]M. Z. Yousaf, J. Yu, Y.-L. Hou, and S. Gao, "Magnetic nanoparticle-based cancer nanodiagnostics," Chin. Phys. B **22**, 058702 (2013).
[21]H. Rui, R. Xing, Z. Xu, Y. Hou, S. Goo, and S. Sun, "Synthesis, functionalization, and biomedical applications of multifunctional magnetic nanoparticles," Adv. Mater. **22**, 2729–2742 (2010).
[22]M. Uhlen, "Magnetic separation of DNA," Nature **340**, 733–734 (1989).
[23]J. Bao, W. Chen, T. Liu, Y. Zhu, P. Jin, L. Wang, J. Liu, Y. Wei, and Y. Li, "Bifunctional au-fe3o4 nanoparticles for protein separation," ACS Nano **1**, 293–298 (2007).
[24]C. Sun, J. S. H. Lee, and M. Zhang, "Magnetic nanoparticles in MR imaging and drug delivery," Adv. Drug Delivery Rev. **60**, 1252–1265 (2008).
[25]H. Chen, T. Moore, B. Qi, D. C. Colvin, E. K. Jelen, D. A. Hitchcock, J. He, O. T. Mefford, J. C. Gore, F. Alexis, and J. N. Anker, "Monitoring pH-triggered drug release from radioluminescent nanocapsules with x-ray excited optical luminescence," ACS Nano **7**, 1178–1187 (2013).
[26]L. Chang, M. Howdyshell, W.-C. Liao, C.-L. Chiang, D. Gallego-Perez, Z. Yang, W. Lu, J. C. Byrd, N. Muthusamy, L. J. Lee, and R. Sooryakumar, "Magnetic tweezers-based 3D microchannel electroporation for high-throughput gene transfection in living cells," Small **11**, 1818–1828 (2014).
[27]J. Devkota, G. Kokkinis, T. Berris, M. Jamalieh, S. Cardoso, F. Cardoso, H. Srikanth, M. H. Phan, and I. Giouroudi, "A novel approach for detection and quantification of magnetic nanomarkers using a spin valve GMR-integrated microfluidic sensor," RSC Adv. **5**, 51169–51175 (2015).
[28]N. Yang and T. Li, "An early cancer diagnosis platform based on micromagnetic sensor array demonstrates ultra-high sensitivity," J. Nanomed. Nanotechnol. **7**, 1000344 (2016).
[29]Y. Wook Jun, Y.-M. Huh, J. sil Choi, J.-H. Lee, H.-T. Song, Kim, S. Yoon, K.-S. Kim, J.-S. Shin, J.-S. Suh, and J. Cheon, "Nanoscale size effect of magnetic nanocrystals and their utilization for cancer diagnosis via magnetic resonance imaging," J. Am. Chem. Soc. **127**, 5732–5733 (2005).
[30]R. V. Roosbroeck, W. V. Roy, T. Stakenborg, J. Trekker, A. D'Hollander, T. Dresselaers, U. Himmelreich, J. Lammertyn, and L. Lagae, "Synthetic antiferromagnetic nanoparticles as potential contrast agents in MRI," ACS Nano **8**, 2269–2278 (2014).
[31]R. Hergt, S. Dutz, R. Müller, and M. Zeisberger, "Magnetic particle hyperthermia: Nanoparticle magnetism and materials development for cancer therapy," J. Phys.: Condens. Matter **18**, S2919–S2934 (2006).
[32]J.-H. Lee, J. tak Jang, J. sil Choi, S. H. Moon, S. hyun Noh, J. wook Kim, J.-G. Kim, I.-S. Kim, K. I. Park, and J. Cheon, "Exchange-coupled magnetic nanoparticles for efficient heat induction," Nat. Nanotechnol. **6**, 418–422 (2011).
[33]S. Dutz, R. Müller, D. Eberbeck, I. Hilger, and M. Zeisberger, "Magnetic nanoparticles adapted for specific biomedical applications," Biomed. Tech. **60**, 405–416 (2015).
[34]D. H. Kim, E. A. Rozhkova, I. V. Ulasov, S. D. Bader, T. Rajh, M. S. Lesniak, and V. Novosad, "Biofunctionalized magnetic-vortex microdiscs for targeted cancer-cell destruction," Nat. Mater. **9**, 165–171 (2010).
[35]R. Mansell, T. Vemulkar, D. C. M. C. Petit, Y. Cheng, J. Murphy, M. S. Lesniak, and R. P. Cowburn, "Magnetic particles with perpendicular anisotropy for mechanical cancer cell destruction," Sci. Rep. **7**, 4257 (2017).
[36]E. A. Vitol, V. Novosad, and E. A. Rozhkova, "Microfabricated magnetic structures for future medicine: From sensors to cell actuators," Nanomedicine **7**, 1611–1624 (2012).
[37]Y. Cheng, M. E. Muroski, D. C. Petit, R. Mansell, T. Vemulkar, R. A. Morshed, Y. Han, I. V. Balyasnikova, C. M. Horbinski, X. Huang, L. Zhang, R. P. Cowburn, and M. S. Lesniak, "Rotating magnetic field induced oscillation of magnetic particles for in vivo mechanical destruction of malignant glioma," J. Controlled Release **223**, 75–84 (2016).
[38]B. Mora, A. Perez-Valle, C. Redondo, M. D. Boyano, and R. Morales, "Cost-effective design of high-magnetic moment nanostructures for biotechnological applications," ACS Appl. Mater. Interfaces **10**, 8165–8172 (2018).
[39]A. Hultgren, M. Tanase, C. Chen, and D. Reich, "High-yield cell separations using magnetic nanowires," IEEE Trans. Magn. **40**, 2988–2990 (2004).
[40]P. C. Pinheiro, C. T. Sousa, J. P. Araújo, A. J. Guiomar, and T. Trindade, "Functionalization of nickel nanowires with a fluorophore aiming at new probes for multimodal bioanalysis," J. Colloid Interface Sci. **410**, 21–26 (2013).
[41]M. Zhang, C. M. Earhart, C. Ooi, R. J. Wilson, M. Tang, and S. X. Wang, "Functionalization of high-moment magnetic nanodisks for cell manipulation and separation," Nano Res. **6**, 745–751 (2013).
[42]D. Shore, S. L. Pailloux, J. Zhang, T. Gage, D. J. Flannigan, M. Garwood, V. C. Pierre, and B. J. H. Stadler, "Electrodeposited fe and fe–au nanowires as MRI contrast agents," Chem. Commun. **52**, 12634–12637 (2016).
[43]M. Bañobre-López, C. Bran, C. Rodríguez-Abreu, J. Gallo, M. Vázquez, and J. Rivas, "A colloidally stable water dispersion of ni nanowires as an efficient t2-MRI contrast agent," J. Mater. Chem. B **5**, 3338–3347 (2017).
[44]M. G. Goikoetxea, "Magnetic vortex nanodiscs for cancer cell destruction," Ph.D. thesis (Universidad Del País Vasco-Euskal Herriko Unibertsitatea, 2017).
[45]T. Shinjo, T. Okuno, R. Hassdorf, K. Shigeto, and T. Ono, "Magnetic vortex core observation in circular dots of permalloy," Science **289**, 930–932 (2000).
[46]K. Y. Guslienko, V. Novosad, Y. Otani, H. Shima, and K. Fukamichi, "Field evolution of magnetic vortex state in ferromagnetic disks," Appl. Phys. Lett. **78**, 3848–3850 (2001).
[47]R. P. Cowburn, D. K. Koltsov, A. O. Adeyeye, M. E. Welland, and D. M. Tricker, "Single-domain circular nanomagnets," Phys. Rev. Lett. **83**, 1042–1045 (1999).
[48]M. Schneider, H. Hoffmann, S. Otto, T. Haug, and J. Zweck, "Stability of magnetic vortices in flat submicron permalloy cylinders," J. Appl. Phys. **92**, 1466–1472 (2002).
[49]J. M. Garcia-Martin, A. Thiaville, J. Miltat, T. Okuno, L. Vila, and L. Piraux, "Imaging magnetic vortices by magnetic force microscopy: Experiments and modelling," J. Phys. D: Appl. Phys. **37**, 965–972 (2004).
[50]V. Novosad, K. Y. Guslienko, H. Shima, Y. Otani, S. G. Kim, K. Fukamichi, N. Kikuchi, O. Kitakami, and Y. Shimada, "Effect of interdot magnetostatic interaction on magnetization reversal in circular dot arrays," Phys. Rev. B **65**, 060402 (2002).
[51]X. Zhu, V. Metlushko, B. Ilic, and P. Grutter, "Direct observation of magnetostatic coupling of chain arrays of magnetic disks," IEEE Trans. Magn. **39**, 2744–2746 (2003).
[52]M. Schneider, H. Hoffmann, and J. Zweck, "Lorentz microscopy of circular ferromagnetic permalloy nanodisks," Appl. Phys. Lett. **77**, 2909 (2000).
[53]K. L. Metlov and K. Y. Guslienko, "Stability of magnetic vortex in soft magnetic nano-sized circular cylinder," J. Magn. Magn. Mater. **242–245**, 1015–1017 (2002).
[54]M. Goiriena-Goikoetxea, K. Y. Guslienko, M. Rouco, I. Orue, E. Berganza, M. Jaafar, A. Asenjo, M. L. Fernández-Gubieda, L. Fernández Barquín, and A. García-Arribasa, "Magnetization reversal in circular vortex dots of small radius," Nanoscale **9**, 11269–11278 (2017).
[55]K. Y. Guslienko and V. Novosad, "Vortex state stability in soft magnetic cylindrical nanodots," J. Appl. Phys. **96**, 4451–4455 (2004).
[56]K. Y. Guslienko, "Magnetic vortex state stability, reversal and dynamics in restricted geometries," J. Nanosci. Nanotechnol. **8**, 2745–2760 (2008).
[57]E. A. Rozhkova, V. Novosad, D. H. Kim, J. Pearson, R. Divan, T. Rajh, and S. D. Bader, "Ferromagnetic microdisks as carriers for biomedical applications," J. Appl. Phys. **105**, 5–8 (2009).
[58]A. Wachowiak, J. Wiebe, M. Bode, O. Pietzsch, M. Morgenstern, and R. Wiesendanger, "Direct observation of internal spin structure of magnetic vortex cores," Science **298**, 577–580 (2002).

[59]P. Szary, "Indication of vortex stabilization and buckling in circular shaped magnetic nanostructures," J. Appl. Phys. **107**, 1–6 (2010).
[60]A. Fernandez and C. J. Cerjan, "Nucleation and annihilation of magnetic vortices in submicron-scale Co dots," J. Appl. Phys. **87**, 1395–1401 (2000).
[61]T. Pokhil, D. Song, and J. Nowak, "Spin vortex states and hysteretic properties of submicron size NiFe elements," J. Appl. Phys. **87**, 6319–6321 (2000).
[62]A. Fernandez, M. Gibbons, M. Wall, and C. Cerjan, "Magnetic domain structure and magnetization reversal in submicron-scale Co dots," J. Magn. Magn. Mater. **190**, 71–80 (1998).
[63]J. S. Neal, H. G. Roberts, M. R. Connolly, S. Crampin, S. J. Bending, G. Wastlbauer, and J. A. Bland, "Magnetisation reversal in epitaxial Fe(1 0 0) disks studied by high resolution scanning Hall probe microscopy," Ultramicroscopy **106**, 614–619 (2006).
[64]L. J. Heyderman, H. H. Solak, C. David, D. Atkinson, R. P. Cowburn, and F. Nolting, "Arrays of nanoscale magnetic dots: Fabrication by x-ray interference lithography and characterization," Appl. Phys. Lett. **85**, 4989–4991 (2004).
[65]X. Zhu, P. Grütter, V. Metlushko, and B. Ilic, "Magnetization reversal and configurational anisotropy of dense permalloy dot arrays," Appl. Phys. Lett. **80**, 4789–4791 (2002).
[66]B. V. Waeyenberge, A. Puzic, H. Stoll, K. W. Chou, T. Tyliszczak, R. Hertel, M. Fähnle, H. Brückl, K. Rott, G. Reiss, I. Neudecker, D. Weiss, C. H. Back, and G. Schütz, "Magnetic vortex core reversal by excitation with short bursts of an alternating field," Nature **444**, 461–464 (2006).
[67]J. Mejía-López, D. Altbir, A. H. Romero, X. Batlle, I. V. Roshchin, C.-P. Li, and I. K. Schuller, "Vortex state and effect of anisotropy in sub-100-nm magnetic nanodots," J. Appl. Phys. **100**, 104319 (2006).
[68]K. Y. Guslienko, V. Novosad, Y. Otani, H. Shima, and K. Fukamichi, "Magnetization reversal due to vortex nucleation, displacement, and annihilation in submicron ferromagnetic dot arrays," Phys. Rev. B **65**, 244141–2441410 (2002).
[69]A. Koh, W. Hu, R. Wilson, S. Wang, and R. Sinclair, "Preparation, structural and magnetic characterization of synthetic anti-ferromagnetic (SAF) nanoparticles," Philos. Mag. **88**, 4225–4241 (2008).
[70]S. Leulmi, H. Joisten, T. Dietsch, C. Iss, M. Morcrette, S. Auffret, P. Sabon, and B. Dieny, "Comparison of dispersion and actuation properties of vortex and synthetic antiferromagnetic particles for biotechnological applications," Appl. Phys. Lett. **103**, 132412 (2013).
[71]T. Vemulkar, R. Mansell, D. C. M. C. Petit, R. P. Cowburn, and M. S. Lesniak, "Highly tunable perpendicularly magnetized synthetic antiferromagnets for biotechnology applications," Appl. Phys. Lett. **107**, 012403 (2015).
[72]W. Hu, R. J. Wilson, A. Koh, A. Fu, A. Z. Faranesh, C. M. Earhart, S. J. Osterfeld, S.-J. Han, L. Xu, S. Guccione, R. Sinclair, and S. X. Wang, "High-moment antiferromagnetic nanoparticles with tunable magnetic properties," Adv. Mater. **20**, 1479–1483 (2008).
[73]W. Hu, R. J. Wilson, C. M. Earhart, A. L. Koh, R. Sinclair, and S. X. Wang, "Synthetic antiferromagnetic nanoparticles with tunable susceptibilities," J. Appl. Phys. **105**, 07B508 (2009).
[74]P. Grünberg, R. Schreiber, Y. Pang, M. B. Brodsky, and H. Sowers, "Layered magnetic structures: Evidence for antiferromagnetic coupling of fe layers across cr interlayers," Phys. Rev. Lett. **57**, 2442–2445 (1986).
[75]S. S. P. Parkin, N. More, and K. P. Roche, "Oscillations in exchange coupling and magnetoresistance in metallic superlattice structures: Co/Ru, Co/Cr, and Fe/Cr," Phys. Rev. Lett. **64**, 2304–2307 (1990).
[76]S. S. P. Parkin, "Systematic variation of the strength and oscillation period of indirect magnetic exchange coupling through the 3d, 4d, and 5d transition metals," Phys. Rev. Lett. **67**, 3598–3601 (1991).
[77]P. Bruno and C. Chappert, "Ruderman-kittel theory of oscillatory interlayer exchange coupling," Phys. Rev. B **46**, 261–270 (1992).
[78]R. A. Duine, K.-J. Lee, S. S. P. Parkin, and M. D. Stiles, "Synthetic antiferromagnetic spintronics," Nat. Phys. **14**, 217–219 (2018).
[79]M. N. Baibich, J. M. Broto, A. Fert, F. N. V. Dau, F. Petroff, P. Etienne, G. Creuzet, A. Friederich, and J. Chazelas, "Giant magnetoresistance of (001)fe/(001)cr magnetic superlattices," Phys. Rev. Lett. **61**, 2472–2475 (1988).
[80]E. E. Fullerton, D. T. Margulies, M. E. Schabes, M. Carey, B. Gurney, A. Moser, M. Best, G. Zeltzer, K. Rubin, H. Rosen, and M. Doerner, "Antiferromagnetically coupled magnetic media layers for thermally stable high-density recording," Appl. Phys. Lett. **77**, 3806–3808 (2000).
[81]S. Byeon, A. Misra, and W. Doyle, "Synthetic antiferromagnetic soft underlayers for perpendicular recording media," IEEE Trans. Magn. **40**, 2386–2388 (2004).
[82]S. Pietambaram, J. Janesky, R. Dave, J. Sun, G. Steiner, and J. Slaughter, "Exchange coupling control and thermal endurance of synthetic antiferromagnet structures for MRAM," IEEE Trans. Magn. **40**, 2619–2621 (2004).
[83]M. Milyaev, L. Naumova, T. Chernyshova, V. Proglyado, I. Kamensky, and V. Ustinov, "Spin-flop in synthetic antiferromagnet and anhysteretic magnetic reversal in FeMn-based spin valves," IEEE Trans. Magn. **52**, 1–4 (2016).
[84]C. D. G. B. D. Cullity, *Introduction to Magnetic Materials*, 2nd ed. (Wiley-IEEE Press, 2008).
[85]Q. L. Vuong, J.-F. Berret, J. Fresnais, Y. Gossuin, and O. Sandre, "A universal scaling law to predict the efficiency of magnetic nanoparticles as MRI t2-contrast agents," Adv. Healthcare Mater. **1**, 502–512 (2012).
[86]R. Lavrijsen, A. Fernández-Pacheco, D. Petit, R. Mansell, J. H. Lee, and R. P. Cowburn, "Tuning the interlayer exchange coupling between single perpendicularly magnetized CoFeB layers," Appl. Phys. Lett. **100**, 052411 (2012).
[87]R. M. Fratila, S. Rivera-Fernández, and J. M. de la Fuente, "Shape matters: Synthesis and biomedical applications of high aspect ratio magnetic nanomaterials," Nanoscale **7**, 8233–8260 (2015).
[88]E. C. Stoner and E. P. Wohlfarth, "A mechanism of magnetic hysteresis in heterogeneous alloys," Philos. Trans. R. Soc., A **240**, 599–642 (1948).
[89]E. H. Frei, S. Shtrikman, and D. Treves, "Critical size and nucleation field of ideal ferromagnetic particles," Phys. Rev. **106**, 446–455 (1957).
[90]A. Arrott, B. Heinrich, and A. Aharoni, "Point singularities and magnetization reversal in ideally soft ferromagnetic cylinders," IEEE Trans. Magn. **15**, 1228–1235 (1979).
[91]C. T. Sousa, D. C. Leitao, M. P. Proenca, J. Ventura, A. M. Pereira, and J. P. Araújo, "Nanoporous alumina as templates for multifunctional applications," Appl. Phys. Rev. **1**, 031102 (2014).
[92]S. Ishrat, K. Maaz, K.-J. Lee, M.-H. Jung, and G.-H. Kim, "Fabrication and temperature-dependent magnetic properties of one-dimensional multilayer Au–Ni–Au–Ni–Au nanowires," J. Solid State Chem. **210**, 116–120 (2014).
[93]L. Liu, W.-Y. Zhou, S.-S. Xie, O. Albrecht, and K. Nielsch, "Microstructure and temperature-dependent magnetic properties of co/pt multilayered nanowires," Chem. Phys. Lett. **466**, 165–169 (2008).
[94]T. Böhnert, A. C. Niemann, A.-K. Michel, S. Bäßler, J. Gooth, B. G. Tóth, K. Neuróhr, L. Péter, I. Bakonyi, V. Vega, V. M. Prida, and K. Nielsch, "Magnetothermopower and magnetoresistance of single Co-Ni/Cu multilayered nanowires," Phys. Rev. B **90**, 165416 (2014).
[95]M. Susano, M. P. Proenca, S. Moraes, C. T. Sousa, and J. P. Araújo, "Tuning the magnetic properties of multisegmented Ni/Cu electrodeposited nanowires with controllable Ni lengths," Nanotechnology **27**, 10 (2016).
[96]S. Moraes, D. Navas, F. Béron, M. Proenca, K. Pirota, C. Sousa, and J. Araújo, "The role of Cu length on the magnetic behaviour of Fe/Cu multi-segmented nanowires," Nanomaterials **8**, 490 (2018).
[97]W. Wernsdorfer, B. Doudin, D. Mailly, K. Hasselbach, A. Benoit, J. Meier, J. P. Ansermet, and B. Barbara, "Nucleation of magnetization reversal in individual nanosized nickel wires," Phys. Rev. Lett. **77**, 1873–1876 (1996).
[98]R. Ferré, K. Ounadjela, J. M. George, L. Piraux, and S. Dubois, "Magnetization processes in nickel and cobalt electrodeposited nanowires," Phys. Rev. B **56**, 14066–14075 (1997).
[99]M. P. Proenca, K. J. Merazzo, L. G. Vivas, D. C. Leitao, C. T. Sousa, J. Ventura, J. P. Araújo, and M. Vazquez, "Co nanostructures in ordered templates: Comparative FORC analysis," Nanotechnology **24**, 475703 (2013).
[100]R. Hertel, "Micromagnetic simulations of magnetostatically coupled nickel nanowires," J. Appl. Phys. **90**, 5752–5758 (2001).
[101]R. Hertel and J. Kirschner, "Magnetization reversal dynamics in nickel nanowires," Physica B **343**, 206–210 (2004).
[102]G. J. Strijkers, J. H. J. Dalderop, M. A. A. Broeksteeg, H. J. M. Swagten, and W. J. M. de Jonge, "Structure and magnetization of arrays of electrodeposited co wires in anodic alumina," J. Appl. Phys. **86**, 5141–5145 (1999).
[103]R. Metzger, V. Konovalov, M. Sun, T. Xu, G. Zangari, B. Xu, M. Benakli, and W. Doyle, "Magnetic nanowires in hexagonally ordered pores of alumina," IEEE Trans. Magn. **36**, 30–35 (2000).

[104]S. Pignard, G. Goglio, A. Radulescu, L. Piraux, S. Dubois, A. Declémy, and J. L. Duvail, "Study of the magnetization reversal in individual nickel nanowires," J. Appl. Phys. **87**, 824–829 (2000).

[105]K. Nielsch, R. B. Wehrspohn, J. Barthel, J. Kirschner, U. Gisele, S. F. Fischer, and H. Kronmüller, "Hexagonally ordered 100 nm period nickel nanowire arrays," Appl. Phys. Lett. **79**, 1360–1362 (2001).

[106]L.-P. Carignan, M. Massicotte, C. Caloz, A. Yelon, and D. Menard, "Magnetization reversal in arrays of ni nanowires with different diameters," IEEE Trans. Magn. **45**, 4070–4073 (2009).

[107]S. Pal, S. Saha, D. Polley, and A. Barman, "Magnetization reversal dynamics in co nanowires with competing magnetic anisotropies," Solid State Commun. **151**, 1994–1998 (2011).

[108]L.-P. Carignan, C. Lacroix, A. Ouimet, M. Ciureanu, A. Yelon, and D. Ménard, "Magnetic anisotropy in arrays of ni, CoFeB, and ni/cu nanowires," J. Appl. Phys. **102**, 023905 (2007).

[109]D. C. Leitao, A. V. Silva, R. Ferreira, E. Paz, F. L. Deepack, S. Cardoso, and P. P. Freitas, "Linear nanometric tunnel junction sensors with exchange pinned sensing layer," J. Appl. Phys. **115**, 17E526 (2014).

[110]D. C. Leitao, J. Ventura, C. T. Sousa, A. M. Pereira, J. B. Sousa, M. Vazquez, and J. P. Araújo, "Insights into the role of magnetoelastic anisotropy in the magnetization reorientation of magnetic nanowires," Phys. Rev. B **84**, 014410 (2011).

[111]H. Xiang, D. M. Jiang, J. C. Yao, Y. P. Zheng, W. Lu, G. Q. Li, H. Saito, S. Ishio, X. W. Tan, and Y. Q. Lin, "Micromagnetic simulations of magnetization reversal of iron nanowire," J. Phys.: Conf. Ser. **266**, 012022 (2011).

[112]X. F. Qin, C. H. Deng, Y. Liu, X. J. Meng, J. Q. Zhang, F. Wang, and X. H. Xu, "Magnetization reversal of high aspect ratio iron nanowires grown by electrodeposition," IEEE Trans. Magn. **48**, 3136–3139 (2012).

[113]Y. P. Ivanov, M. Vázquez, and O. Chubykalo-Fesenko, "Magnetic reversal modes in cylindrical nanowires," J. Phys. D: Appl. Phys. **46**, 485001 (2013).

[114]Y. Gao, Y. Liu, and, and C. Xu, "Magnetic nanoparticles for biomedical applications: From diagnosis to treatment to regeneration," *Engineering in Translational Medicine* (Springer London, 2013), pp. 567–583.

[115]P. E. Garcia Casillas, I. Olivas-Armendariz, C. Gonzalez, K. Castrejon-Parga, and C. Martinez Perez, "Microspheres technologies, applications and role in drug delivery systems," Magnetic Nanostructures for Biomedical Applications (NOVA, 2014), pp. 137–180.

[116]N. Tran and T. J. Webster, "Magnetic nanoparticles: Biomedical applications and challenges," J. Mater. Chem. **20**, 8760 (2010).

[117]H. Chiriac, E. Radu, M. Tibu, G. Stoian, G. Ababei, L. Lăbuşcă, D.-D. Herea, and N. Lupu, "Fe-Cr-Nb-B ferromagnetic particles with shape anisotropy for cancer cell destruction by magneto-mechanical actuation," Sci. Rep. **8**, 11538 (2018).

[118]K. Wu, D. Su, J. Liu, and J.-P. Wang, "Estimating saturation magnetization of superparamagnetic nanoparticles in liquid phase," J. Magn. Magn. Mater. **471**, 394–399 (2019).

[119]*Nanogels for Biomedical Applications*, edited by A. Vashist, A. K. Kaushik, S. Ahmad, and M. Nair (Royal Society of Chemistry, 2017).

[120]E. D. B. Paola Palmero and F. Cambier, *Advances in Ceramic Biomaterials* (Elsevier Science & Technology, 2017).

[121]E. C. Wang and A. Z. Wang, "Nanoparticles and their applications in cell and molecular biology," Integr. Biol. **6**, 9–26 (2013).

[122]N. Gao, H. Wang, and E.-H. Yang, "An experimental study on ferromagnetic nickel nanowires functionalized with antibodies for cell separation," Nanotechnology **21**, 105107 (2010).

[123]*Plasmonics: Theory and Applications*, edited by, T. V. Shahbazyan and M. I. Stockman (Springer Netherlands, 2013).

[124]B. D. Plouffe, S. K. Murthy, and L. H. Lewis, "Fundamentals and application of magnetic particles in cell isolation and enrichment: A review," Rep. Prog. Phys. **78**, 016601 (2014).

[125]R. Burger and J. Ducrée, "Handling and analysis of cells and bioparticles on centrifugal microfluidic platforms," Expert Rev. Mol. Diagn. **12**, 407–421 (2012).

[126]B. D. Plouffe and S. K. Murthy, "Perspective on microfluidic cell separation: A solved problem?," Anal. Chem. **86**, 11481–11488 (2014).

[127]B. Zhu and S. K. Murthy, "Stem cell separation technologies," Curr. Opin. Chem. Eng. **2**, 3–7 (2013).

[128]C. Ruffert, "Magnetic bead—magic bullet," Micromachines **7**, 21 (2016).

[129]B. J. Kirby, *Micro- And Nanoscale Fluid Mechanics* (Cambridge University Press, 2010).

[130]Y. P. Ivanov, A. Alfadhel, M. Alnassar, J. E. Perez, M. Vazquez, A. Chuvilin, and J. Kosel, "Tunable magnetic nanowires for biomedical and harsh environment applications," Sci. Rep. **6**, 24189 (2016).

[131]A. Hultgren, M. Tanase, C. S. Chen, G. J. Meyer, and D. H. Reich, "Cell manipulation using magnetic nanowires," J. Appl. Phys. **93**, 7554–7556 (2003).

[132]D. H. Reich, M. Tanase, A. Hultgren, L. A. Bauer, C. S. Chen, and G. J. Meyer, "Biological applications of multifunctional magnetic nanowires (invited)," J. Appl. Phys. **93**, 7275–7280 (2003).

[133]A. Hultgren, M. Tanase, E. J. Felton, K. Bhadriraju, A. K. Salem, C. S. Chen, and D. H. Reich, "Optimization of yield in magnetic cell separations using nickel nanowires of different lengths," Biotechnol. Prog. **21**, 509–515 (2008).

[134]R. E. McMahon, J. Ma, S. V. Verkhoturov, D. Munoz-Pinto, I. Karaman, F. Rubitschek, H. J. Maier, and M. S. Hahn, "A comparative study of the cytotoxicity and corrosion resistance of nickel–titanium and titanium–niobium shape memory alloys," Acta Biomater. **8**, 2863–2870 (2012).

[135]F. Byrne, A. Prina-Mello, A. Whelan, B. M. Mohamed, A. Davies, Y. K. Gun'ko, J. Coey, and Y. Volkov, "High content analysis of the biocompatibility of nickel nanowires," J. Magn. Magn. Mater. **321**, 1341–1345 (2009).

[136]L. P. Felix, J. E. Perez, M. F. Contreras, T. Ravasi, and J. Kosel, "Cytotoxic effects of nickel nanowires in human fibroblasts," Toxicology Rep. **3**, 373–380 (2016).

[137]N. Alsharif, "Towards the generation of functionalized magnetic nanowires to target leukemic cells," Master's thesis (King Abdullah University of Science and Technology, 2016).

[138]N. A. Alsharif, A. Martiinez-Banderas, J. Merzaban, T. Ravasi, and J. Kosel, "Biofunctionalizing magnetic nanowires toward targeting and killing leukemia cancer cells," IEEE Trans. Magn. **55**, 1–5 (2019).

[139]A. Fu, W. Hu, L. Xu, R. Wilson, H. Yu, S. Osterfeld, S. Gambhir, and S. Wang, "Protein-functionalized synthetic antiferromagnetic nanoparticles for biomolecule detection and magnetic manipulation," Angew. Chem. Int. Ed. **48**, 1620–1624 (2009).

[140]M. Hayden and P.-J. Nacher, *History and physical principles of MRI. Luca SABA. Magnetic Resonance Imaging Handbook* (CRC Press, 2016), Vol. 1.

[141]G. Placidi, *MRI: Essentials for Innovative Technologies* (CRC Press, 2012).

[142]P. W. Stroman, *Essentials of Functional MRI* (CRC Press, 2016).

[143]S. Aja-Fernández and G. Vegas-Sánchez-Ferrero, *Statistical Analysis of Noise in MRI* (Springer International Publishing, 2016).

[144]G. Karunamuni, *The Cardiac Lymphatic System* (Springer New York, 2013).

[145]S. A. Corr, S. J. Byrne, R. Tekoriute, C. J. Meledandri, D. F. Brougham, M. Lynch, C. Kerskens, L. O'Dwyer, and Y. K. Gun'ko, "Linear assemblies of magnetic nanoparticles as MRI contrast agents," J. Am. Chem. Soc. **130**, 4214–4215 (2008).

[146]J. W. Bulte and M. D. Cuyper, "Magnetoliposomes as contrast agents," *Liposomes, Part C* (Elsevier, 2003), pp. 175–198.

[147]J. Lee, *Computed Body Tomography with MRI Correlation* (Wolters Kluwer Health, 2005).

[148]D. T. Yashwant Pathak, *Drug Delivery Nanoparticles Formulation and Characterization (Drugs and the Pharmaceutical Sciences Book 191)* (CRC Press, 2016).

[149]B. H. Raymond, Y. Kwong, and M. Jerosch-Herold, *Cardiovascular Magnetic Resonance Imaging* (Springer-Verlag GmbH, 2019).

[150]Y.-D. Xiao, R. Paudel, J. Liu, C. Ma, Z.-S. Zhang, and S.-K. Zhou, "MRI contrast agents: Classification and application (review)," Int. J. Mol. Med. **38**, 1319–1326 (2016).

[151]X. Chen and S. Wong, *Cancer Theranostics* (Elsevier Science Publishing Co Inc, 2014).

[152]A. Merbach, L. Helm, and É. Tóth, eds., *The Chemistry of Contrast Agents in Medical Magnetic Resonance Imaging* (John Wiley & Sons, Ltd, 2013).

[153]H.-K. Kim, G. H. Lee, and Y. Chang, "Gadolinium as an MRI contrast agent," Future Med. Chem. **10**, 639–661 (2018).

[154]M. Rogosnitzky and S. Branch, "Gadolinium-based contrast agent toxicity: A review of known and proposed mechanisms," BioMetals **29**, 365–376 (2016).

[155]J. Ramalho, R. C. Semelka, M. Ramalho, R. H. Nunes, M. AlObaidy, and M. Castillo, "Gadolinium-based contrast agent accumulation and toxicity: An update," Am. J. Neuroradiol. **37**, 1192–1198 (2015).
[156]Z. Zhou and Z.-R. Lu, "Gadolinium-based contrast agents for magnetic resonance cancer imaging," Wiley Interdiscip. Rev.: Nanomed. Nanobiotechnol. **5**, 1–18 (2012).
[157]A.-H. Lu, E. Salabas, and F. Schüth, "Magnetic nanoparticles: Synthesis, protection, functionalization, and application," Angew. Chem. Int. Ed. **46**, 1222–1244 (2007).
[158]D. Andrews, T. Nann, and R. Lipson, *Comprehensive Nanoscience and Nanotechnology* (Academic Press, 2019).
[159]Q. L. Vuong, P. Gillis, and Y. Gossuin, "Monte carlo simulation and theory of proton NMR transverse relaxation induced by aggregation of magnetic particles used as MRI contrast agents," J. Magn. Reson. **212**, 139–148 (2011).
[160]L. Li, W. Jiang, K. Luo, H. Song, F. Lan, Y. Wu, and Z. Gu, "Superparamagnetic iron oxide nanoparticles as MRI contrast agents for non-invasive stem cell labeling and tracking," Theranostics **3**, 595–615 (2013).
[161]M. J. Bailey, R. van der Weegen, P. J. Klemm, S. L. Baker, and B. A. Helms, "Stealth rare earth oxide nanodiscs for magnetic resonance imaging," Adv. Healthcare Mater. **1**, 437–442 (2012).
[162]V. Jacques, S. Dumas, W.-C. Sun, J. S. Troughton, M. T. Greenfield, and P. Caravan, "High-relaxivity magnetic resonance imaging contrast agents part 2," Invest. Radiol. **45**, 613–624 (2010).
[163]G. Singh, B. H. McDonagh, S. Hak, D. Peddis, S. Bandopadhyay, I. Sandvig, A. Sandvig, and W. R. Glomm, "Synthesis of gadolinium oxide nanodisks and gadolinium doped iron oxide nanoparticles for mr contrast agents," J. Mater. Chem. B **5**, 418–422 (2017).
[164]T. Peci, "Carbon nanotubes lled with continuous ferromagnetic-Fe nanowires and surface-functionalized with paramagnetic Gd(III): A candidate magnetic hyperthermia structure and MRI contrast agent," Ph.D. thesis (Queen Mary University of London, 2017).
[165]K. Cham-Fai and Y.-X. J. Wang, "Mn–Fe nanowires towards cell labeling and magnetic resonance imaging," *Nanowires Science and Technology* (InTech, 2010).
[166]H. Na, J. Lee, K. An, Y. Park, M. Park, I. Lee, D.-H. Nam, S. Kim, S.-H. Kim, S.-W. Kim, K.-H. Lim, K.-S. Kim, S.-O. Kim, and T. Hyeon, "Development of aT1 contrast agent for magnetic resonance imaging using MnO nanoparticles," Angew. Chem. **119**, 5493–5497 (2007).
[167]H. R. Neves, R. A. Bini, J. H. O. Barbosa, C. E. G. Salmon, and L. C. Varanda, "Dextran-coated antiferromagnetic MnO nanoparticles for aT1-MRI contrast agent with high colloidal stability," Part. Part. Syst. Charact. **33**, 167–176 (2016).
[168]Y.-K. Peng, C.-L. Liu, H.-C. Chen, S.-W. Chou, W.-H. Tseng, Y.-J. Tseng, C.-C. Kang, J.-K. Hsiao, and P.-T. Chou, "Antiferromagnetic iron nanocolloids: A new generation in vivo t1 MRI contrast agent," J. Am. Chem. Soc. **135**, 18621–18628 (2013).
[169]A. I. Martínez-Banderas, A. Aires, F. J. Teran, J. E. Perez, J. F. Cadenas, N. Alsharif, T. Ravasi, A. L. Cortajarena, and J. Kosel, "Functionalized magnetic nanowires for chemical and magneto-mechanical induction of cancer cell death," Sci. Rep. **6**, 1–11 (2016).
[170]D. W. Wong, W. L. Gan, N. Liu, and W. S. Lew, "Magneto-actuated cell apoptosis by biaxial pulsed magnetic field," Sci. Rep. **7**, 10919 (2017).
[171]S. Leulmi, X. Chauchet, M. Morcrette, G. Ortiz, H. Joisten, P. Sabon, T. Livache, Y. Hou, M. Carrière, S. Lequien, and B. Dieny, "Triggering the apoptosis of targeted human renal cancer cells by the vibration of anisotropic magnetic particles attached to the cell membrane," Nanoscale **7**, 15904–15914 (2015).
[172]N. Wang, "Review of cellular mechanotransduction," J. Phys. D: Appl. Phys. **50**, 233002 (2017).
[173]H. Zabel, *Radiology, Lasers, Nanoparticles and Prosthetics* (Gruyter, Walter de GmbH, 2017).
[174]S. W. Lowe and A. W. Lin, "Apoptosis in cancer," Carcinogenesis **21**, 485–495 (2000).
[175]E. A. Vitol, V. Novosad, and E. A. Rozhkova, "Multifunctional ferromagnetic disks for modulating cell function," IEEE Trans. Magn. **48**, 3269–3274 (2012).
[176]D. Shi, Y. Cheng, M. Chu, and B. Zhang, *The World Scientific Encyclopedia of Nanomedicine and Bioengineering I* (World Scientific, 2015).
[177]X.-L. Liu, Y. Yang, J.-P. Wu, Y.-F. Zhang, H.-M. Fan, and J. Ding, "Novel magnetic vortex nanorings/nanodiscs: Synthesis and theranostic applications," Chin. Phys. B **24**, 127505 (2015).
[178]E. A. Rozhkova, I. V. Ulasov, D. Kim, N. M. Dimitrijevic, V. Novosad, S. D. Bader, M. S. Lesniak, and T. Rajh, "Multifunctional nano-bio materials within cellular machinery," Int. J. Nanoscience **10**, 899–908 (2011).
[179]V. Novosad and E. A. Rozhkova, "Ferromagnets-based multifunctional nanoplatform for targeted cancer therapy," in *Biomedical Engineering, Trends in Materials Science* (InTech, 2011).
[180]M. Goiriena-Goikoetxea, I. Orue, K. Guslienko, E. Berganza, M. Jaafar, A. Asenjo, D. Munoz, A. Muela, and A. Garcia-Arribas, "Properties of permalloy nanodiscs in magnetic vortex state and magneto-mechanical treatment of cancer cells," in *IEEE International Magnetics Conference (INTERMAG)* (IEEE, 2018).
[181]A. O. Fung, V. Kapadia, E. Pierstorff, D. Ho, and Y. Chen, "Induction of cell death by magnetic actuation of nickel nanowires internalized by fibroblasts," J. Phys. Chem. C **112**, 15085–15088 (2008).
[182]D. S. Choi, X. Hopkins, R. Kringel, J. Park, I. T. Jeon, and Y. K. Kim, "Magnetically driven spinning nanowires as effective materials for eradicating living cells," J. Appl. Phys. **111**, 07B329 (2012).
[183]M. Contreras, R. Sougrat, A. Zaher, T. Ravasi, and J. Kosel, "Non-chemotoxic induction of cancer cell death using magnetic nanowires," Int. J. Nanomed. **2015**, 2141–2153.
[184]M. F. Contreras, "Magnetic nanowires as materials for cancer cell destruction," Ph.D. thesis (King Abdullah University of Science and Technology, 2015).
[185]A. Serrà, G. Vázquez-Mariño, J. García-Torres, M. Bosch, and E. Vallés, "Magnetic actuation of multifunctional nanorobotic platforms to induce cancer cell death," Adv. Biosyst. **2**, 1700220 (2018).
[186]B. S. Kwon, "Multilayered magnetic nanoparticles fabricated by nanoimprint lithography for magnetomechanical treatment of cancer," Ph.D. thesis (University of Washington, 2017).
[187]Y. Shen, C. Wu, T. Q. P. Uyeda, G. R. Plaza, B. Liu, Y. Han, M. S. Lesniak, and Y. Cheng, "Elongated nanoparticle aggregates in cancer cells for mechanical destruction with low frequency rotating magnetic field," Theranostics **7**, 1735–1748 (2017).
[188]M. Salimi, S. Sarkar, S. Fathi, A. Alizadeh, R. Saber, F. Moradi, and H. Delavari, "Biodistribution, pharmacokinetics, and toxicity of dendrimer-coated iron oxide nanoparticles in BALB/c mice," Int. J. Nanomed. **13**, 1483–1493 (2018).
[189]N. Hoshyar, S. Gray, H. Han, and G. Bao, "The effect of nanoparticle size on in vivo pharmacokinetics and cellular interaction," Nanomedicine **11**, 673–692 (2016).
[190]J. P. M. Almeida, A. L. Chen, A. Foster, and R. Drezek, "In vivobiodistribution of nanoparticles," Nanomedicine **6**, 815–835 (2011).
[191]B. Pham, E. Colvin, N. Pham, B. Kim, E. Fuller, E. Moon, R. Barbey, S. Yuen, B. Rickman, N. Bryce, S. Bickley, M. Tanudji, S. Jones, V. Howell, and B. Hawkett, "Biodistribution and clearance of stable superparamagnetic maghemite iron oxide nanoparticles in mice following intraperitoneal administration," Int. J. Mol. Sci. **19**, 205 (2018).
[192]Q. Feng, Y. Liu, J. Huang, K. Chen, J. Huang, and K. Xiao, "Uptake, distribution, clearance, and toxicity of iron oxide nanoparticles with different sizes and coatings," Sci. Rep. **8**, 2082 (2018).
[193]C. C. Quini, A. G. Próspero, M. F. Calabresi, G. M. Moretto, N. Zufelato, S. Krishnan, D. R. Pina, R. B. Oliveira, O. Baffa, A. F. Bakuzis, and J. R. Miranda, "Real-time liver uptake and biodistribution of magnetic nanoparticles determined by AC biosusceptometry," Nanomedicine: Nanotechnol., Biol. Med. **13**, 1519–1529 (2017).
[194]Q. Yu, X. qin Xiong, L. Zhao, T. ting Xu, H. Bi, R. Fu, and Q. hua Wang, "Biodistribution and toxicity assessment of superparamagnetic iron oxide nanoparticles in vitro and in vivo," Curr. Med. Sci. **38**, 1096–1102 (2018).
[195]Z. Liu, W. Cai, L. He, N. Nakayama, K. Chen, X. Sun, X. Chen, and H. Dai, "In vivo biodistribution and highly efficient tumour targeting of carbon nanotubes in mice," Nat. Nanotechnol. **2**, 47–52 (2006).
[196]A. A. Faraj, F. Fauvelle, N. Luciani, G. Lacroix, M. Levy, Y. Cremillieux, and E. Canet-Soulas, "In vivo biodistribution and biological impact of injected carbon nanotubes using magnetic resonance techniques," Int. J. Nanomed. **2011**, 351 (2011).

[197]K. Yang and Z. Liu, "In vivo biodistribution, pharmacokinetics, and toxicology of carbon nanotubes," Curr. Drug Metab. **13**, 1057–1067 (2012).
[198]N. R. Jacobsen, P. Møller, P. A. Clausen, A. T. Saber, C. Micheletti, K. A. Jensen, H. Wallin, and U. Vogel, "Biodistribution of carbon nanotubes in animal models," Basic Clin. Pharmacol. Toxicol. **121**, 30–43 (2017).
[199]Z. Liu, S. Tabakman, K. Welsher, and H. Dai, "Carbon nanotubes in biology and medicine: In vitro and in vivo detection, imaging and drug delivery," Nano Res. **2**, 85–120 (2009).
[200]S. tao Yang, W. Guo, Y. Lin, X. yong Deng, H. fang Wang, H. fang Sun, Y. fang Liu, X. Wang, W. Wang, M. Chen, Y. pu Huang, and Y.-P. Sun, "Biodistribution of pristine single-walled carbon nanotubes in vivo†," J. Phys. Chem. C **111**, 17761–17764 (2007).
[201]D. M. Noonan, E. Principi, R. Girardello, A. Bruno, I. Manni, E. Gini, A. Pagani, A. Grimaldi, F. Ivaldi, T. Congiu, D. D. Stefano, G. Piaggio, M. de Eguileor, and A. Albini, "Systemic distribution of single-walled carbon nanotubes in a novel model: alteration of biochemical parameters, metabolic functions, liver accumulation, and inflammation in vivo," Int. J. Nanomed. **11**, 4299–4316 (2016).
[202]Z. Lin, H. Zhang, J. Huang, Z. Xi, L. Liu, and B. Lin, "Biodistribution of single-walled carbon nanotubes in rats," Toxicol. Res. **3**, 497–502 (2013).
[203]P. Huda, T. Binderup, M. C. Pedersen, S. R. Midtgaard, D. R. Elema, A. Kjær, M. Jensen, and L. Arleth, "PET/CT based in vivo evaluation of 64cu labelled nanodiscs in tumor bearing mice," PLOS ONE **10**, e0129310 (2015).
[204]E. Blanco, H. Shen, and M. Ferrari, "Principles of nanoparticle design for overcoming biological barriers to drug delivery," Nat. Biotechnol. **33**, 941–951 (2015).
[205]S. Moghimi, A. Hunter, and T. Andresen, "Factors controlling nanoparticle pharmacokinetics: An integrated analysis and perspective," Annu. Rev. Pharmacol. Toxicol. **52**, 481–503 (2012).
[206]M. Elsabahy and K. L. Wooley, "Design of polymeric nanoparticles for biomedical delivery applications," Chem. Soc. Rev. **41**, 2545 (2012).
[207]P. Decuzzi, B. Godin, T. Tanaka, S.-Y. Lee, C. Chiappini, X. Liu, and M. Ferrari, "Size and shape effects in the biodistribution of intravascularly injected particles," J. Controlled Release **141**, 320–327 (2010).